minerals

MDPI

Article

Application of Multispectral Data in Detecting Porphyry Copper Deposits: The Case of Aidarly Deposit, Eastern Kazakhstan

Elmira Serikbayeva [1,2], Kuanysh Togizov [2,*], Dinara Talgarbayeva [1], Elmira Orynbassarova [2], Nurmakhambet Sydyk [1] and Aigerim Bermukhanova [2]

[1] Institute of Ionosphere, Almaty 050020, Kazakhstan; e.serikbayeva@ionos.kz (E.S.); talgarbayeva.d@ionos.kz (D.T.); nurmakhambet.sydyk@ionos.kz (N.S.)
[2] Department of Geological Survey, Search and Exploration of Mineral Deposits, Satbayev University, Almaty 050013, Kazakhstan; e.orynbassarova@satbayev.university (E.O.); a.bermuhanova@stud.satbayev.university (A.B.)
* Correspondence: k.togizov@satbayev.university; Tel.: +7-7021710995

Abstract

The Koldar Massif in southeastern Kazakhstan is a geologically complex area with potential for porphyry copper and rare-metal mineralization. This study applies a multi-scale remote sensing approach to delineate hydrothermal alteration zones using medium-resolution ASTER imagery and very high-resolution WorldView-3 data. Image processing techniques—including false color composites (FCCs), band ratios (BRs), and the Spectral Angle Mapper (SAM)—were employed across the VNIR and SWIR bands to detect alteration minerals such as kaolinite, illite, montmorillonite, chlorite, epidote, calcite, quartz, and muscovite. These minerals correspond to argillic, propylitic, and phyllic alteration zones. While ASTER supported regional-scale mapping, WorldView-3 enabled detailed analysis at the Aidarly deposit. Validation was performed using copper occurrences, lithogeochemical anomaly contours, and ore body boundaries. The results show a strong spatial correlation between the mapped alteration zones and known mineralization patterns. Importantly, this study reports the identification of a previously undocumented hydrothermal zone north of the Aidarly deposit, detected using WorldView-3 data. This zone exhibits concentric phyllic and argillic alterations, similar to those at Aidarly, and may represent an extension of the mineralized system. Unlike earlier studies on the Aktogay deposit based on ASTER and Landsat-8, this work focuses on the Aidarly deposit and introduces higher-resolution analysis and SAM-based classification, offering improved spatial accuracy and target delineation. The proposed methodology provides a reproducible and scalable workflow for early-stage mineral exploration in underexplored regions, especially where field access is limited. These results highlight the value of high-resolution remote sensing in detecting concealed porphyry copper systems in structurally complex terrains.

Keywords: Koldar Massif; Aidarly deposit; hydrothermal alteration zone; novel hydrothermal zone; ASTER; WorldView 3; copper porphyry mineralization

check for updates

Academic Editor: Stanisław Mazur

Received: 9 June 2025
Revised: 11 August 2025
Accepted: 11 August 2025
Published: 3 September 2025

Citation: Serikbayeva, E.; Togizov, K.; Talgarbayeva, D.; Orynbassarova, E.; Sydyk, N.; Bermukhanova, A. Application of Multispectral Data in Detecting Porphyry Copper Deposits: The Case of Aidarly Deposit, Eastern Kazakhstan. *Minerals* **2025**, *15*, 938. https://doi.org/10.3390/min15090938

Copyright: © 2025 by the authors. Licensee MDPI, Basel, Switzerland. This article is an open access article distributed under the terms and conditions of the Creative Commons Attribution (CC BY) license (https://creativecommons.org/licenses/by/4.0/).

1. Introduction

Porphyry copper deposits are globally recognized as the primary sources of copper, along with significant by-products such as molybdenum, gold, and silver. These deposits are typically large, low-grade systems (0.3%–2.0% Cu) and play a critical role in sustaining the global copper supply chain, which underpins modern infrastructure and technological development [1–4]. Their significance has grown in recent decades due to the increasing

demand for copper in electrical applications, renewable energy systems, and industrial manufacturing [5,6].

Porphyry copper deposits form through the circulation of hydrothermal fluids triggered by magmatic intrusions into host rocks [7–9]. These systems are typically associated with well-developed hydrothermal alteration zones, containing minerals with diagnostic spectral absorption features [4,10]. This makes them suitable targets for satellite-based remote sensing, which can aid in mapping alteration zones and inferring subsurface mineralization [11].

Kazakhstan is endowed with a wealth of mineral resources, among which porphyry copper deposits hold particular significance due to their scale, economic value, and strategic importance. Notable deposits such as Aktogay, Aidarly, Kyzylkiya, Bozshakol, and Koksai represent some of the most prominent porphyry systems in the region. These deposits are typically characterized by extensive hydrothermal alteration zones, which are key indicators of mineralization and are critical for exploration and resource assessment. The development and exploitation of these deposits have played a vital role in bolstering Kazakhstan's mining sector, contributing substantially to the national economy and reinforcing the country's position as a major contributor to the global supply of copper and other base metals [11–14]. Despite this considerable mineral potential and the economic importance of porphyry systems, the application of advanced geospatial technologies, particularly remote sensing, remains relatively limited in Kazakhstan.

The Koldar Massif in eastern Kazakhstan is a geologically complex area with favorable conditions for porphyry-style mineralization. It is characterized by extensive structural deformation, hydrothermal overprint, and multiple copper occurrences. A recent systematic study [3,15–17] provided a regional-scale assessment of the Koldar Massif using ASTER and Landsat data, focusing primarily on large deposits such as Aktogay [15]. While that study served as a reconnaissance-level investigation, the current research builds upon and extends it by implementing a hierarchical remote sensing workflow tailored to the scale and resolution needed for effective mineral exploration at Aidarly. Both studies employed similar spectral techniques such as band ratios (BRs) and false color composites (FCCs); however, our study introduces the Spectral Angle Mapper (SAM) algorithm for more targeted classification. Rather than treating sensors equally, we integrate their individual strengths: ASTER for the initial mapping and WorldView-3 for detailed mineralogical refinement and validation.

Furthermore, we enhance the result validation by overlaying copper occurrences, lithogeochemical anomaly contours, and ore body boundaries, allowing for a more accurate visual and spatial assessment of the consistency between detected alteration zones and known mineralization. This multi-resolution and multi-validation approach improves the reliability of hydrothermal mapping and enables more confident delineation of concealed mineralized systems, even in areas with restricted access. In this regard, our work reports the discovery of a previously undocumented hydrothermal zone north of the Aidarly deposit. This zone, identified via WorldView-3 imagery, exhibits concentric phyllitic and argillic alterations similar to those at Aidarly, suggesting a possible extension of the mineralized system.

Conventional exploration methods in such terrains face several challenges, including limited surface exposure, thick overburden, and difficult access. These factors increase exploration costs and timelines. In contrast, satellite-based remote sensing offers a cost-effective, scalable, and non-invasive approach to target generation in poorly accessible or underexplored regions [18–21]. Over the past decades, multispectral and hyperspectral remote sensing sensors have been widely employed in mineral exploration across various geological settings [20,22–25].

The Advanced Spaceborne Thermal Emission and Reflection Radiometer (ASTER) has proven effective in identifying hydroxyl- and iron-bearing minerals through its VNIR and SWIR bands, aiding the detection of alteration zones [26,27]. More recently, WorldView-3, with its very high spatial and spectral resolution, has enabled more detailed lithological mapping and mineral detection in hydrothermally altered terrains [28–30]. Several comparative studies have shown the superior mineral-mapping capabilities of WorldView-3 relative to ASTER [31–36].

However, despite the proven capabilities of high-resolution sensors such as WorldView-3 for mapping key alteration minerals, their application in Kazakhstan remains limited.

The main objective of this study is to utilize the strengths of multispectral remote sensing data to delineate the hydrothermal alteration zones associated with porphyry copper mineralization at the regional and local scales. Specifically, we aim (1) to map the hydrothermal alteration zones in the Aidarly deposit using ASTER and WorldView-3 based on their respective spectral advantages; (2) to apply the FCC, BR, and SAM techniques for the accurate classification of alteration minerals; and (3) to validate the results using lithogeochemical maps, field sampling points, and copper occurrences. This approach demonstrates how optimal sensor integration can enhance porphyry copper exploration in eastern Kazakhstan. The approach presented here can serve as a practical framework for remote sensing-based mineral exploration in other underexplored regions, supporting more efficient targeting of porphyry copper deposits and contributing to the broader application of geospatial technologies in mineral resource development.

2. Geographical and Geological Settings

The Aidarly–Aktogay group of deposits is located in the Abay region, Ayagoz district, 25 km east of the Aktogay railway station. The distance between the Aktogay and Aidarly deposits is approximately 3 km (Figure 1). The region is characterized by a moderately continental climate with hot summers and cold winters. The terrain is gently rolling, with elevations ranging from 400 to 600 m, and the vegetation is semi-desert. Geologically, the deposit belongs to the Dzungar–Balkhash structural–formational zone [2]. Permanent watercourses are absent, and the water supply is provided by seasonal streams and underground sources. The vegetation is sparse, consisting of steppe and semi-desert species such as feather grass, wormwood, and saxaul [14].

Geologically, Aidarly, Aktogay, and Kyzylkiya are large copper porphyry deposits associated with granitoid intrusions of the late Paleozoic age [2]. The main rocks in the area include granodiorites and quartz diorites, as well as volcanogenic sedimentary rocks such as tuffs, tuffaceous sandstones, and schists.

The Aidarly deposit is one of the largest copper porphyry deposits in Kazakhstan and has significant reserves of 1.53 billion tons of ore with a copper content of 0.38%, as well as gold (14.14 tons), silver (2.17 thousand tons), and molybdenum (154.28 thousand tons) [37].

The deposit was discovered by the Alma-Ata party based on earlier induced polarization (IP) survey data and the study of secondary copper and molybdenum scattering halos, which were obtained in 1974 as a result of a 1:50,000 scale geological survey (Figure 2). During the same period, detailed route observations and prospecting work were carried out in the area of the anomalies. According to the results from their evaluation by geologist Belykh L.P., it was established that there was copper mineralization, as well as single ore outcrops, at the contact with dikes of quartz or plagiogranite granodiorite porphyries. Thus, the nature of the ER anomaly and scattering halos was proven [38].

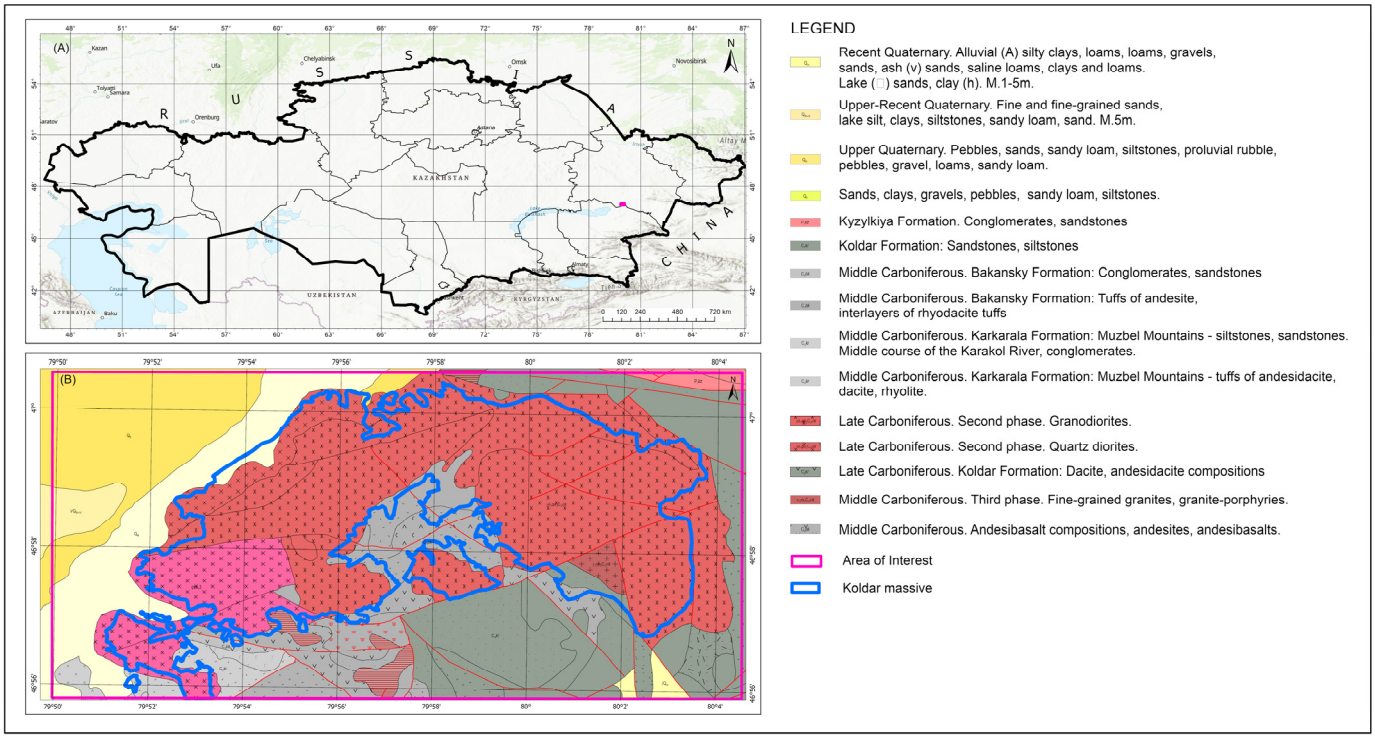


Figure 1. (**A**) The regional geographical location of the study area and surrounding regions compiled from ArcMap basemaps, and (**B**) a simplified geological map of the study area.

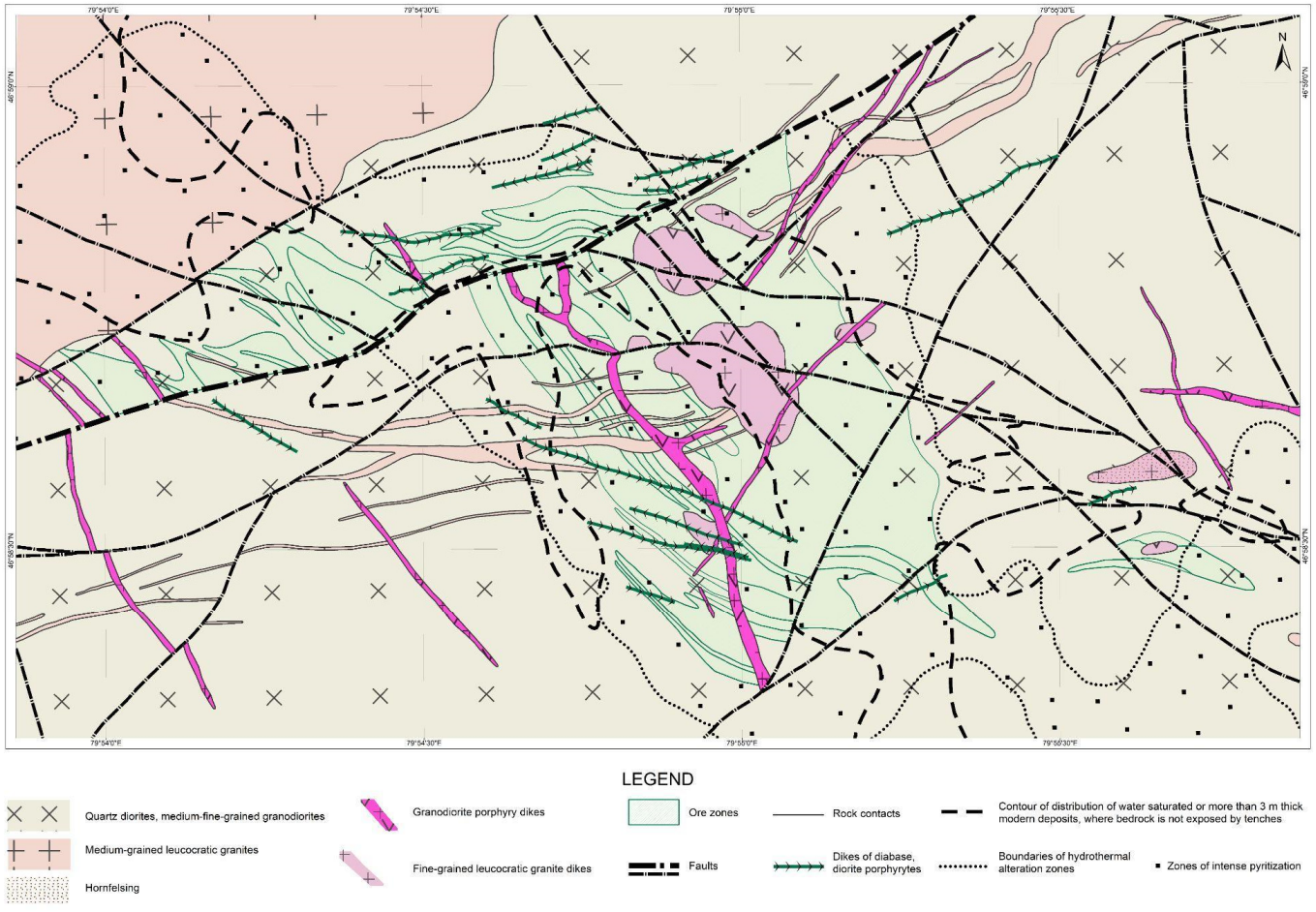


Figure 2. Detailed geological map of the Aidarly deposit.

The site is covered by aeolian loams and is difficult to study from the surface. In 1975, 1:10,000 scale-induced polarization, magnetic, gravity, and lithochemical surveys were carried out at the site. As a result of these works, the Aidarly deposit was highlighted by contrasting copper and molybdenum scattering halos and the associated induced polarization anomalies, allowing the area of distribution of molybdenum–copper mineralization to be determined.

The Aidarly deposit, in terms of the composition and zonality of the hydrothermal alterations and mineralization, is no different from most other porphyry copper deposits worldwide. The area features sections of the spatially associated manifestations of two stages of propylitization—epidote–amphibole and albite–prehnite–chlorite; alkaline metasomatism—biotitization and quartz–potassium feldspar alterations; the acid leaching stage—argillization, the development of anhydrite, and quartz–sericite metasomatism; the borosilicate stage—tourmalinization; and the late alkaline stage—carbonatization and zeolitization of plagioclase [11].

Ore bodies at the deposits are associated with the central parts of granitoid intrusions and are represented by veins, lenses, and fractured zones enriched with copper–molybdenum minerals. Primary ore minerals include chalcopyrite, bornite, molybdenite, and pyrite. Accompanying minerals may include galena, sphalerite, and magnetite. Metasomatic alterations, such as propylitization, argillization, and quartzitization, are widespread, indicating intense hydrothermal activity in the area [39,40].

Structurally, the Aidarly deposit is located in the western part of the Koldar intrusive anticlinorium. Geographical accessibility and large reserves of copper, molybdenum, and related elements make this deposit promising for long-term development. However, it is necessary to take into account environmental aspects and introduce modern technologies to ensure efficient ore extraction with minimal environmental impact.

3. Materials and Methods

In order to validate the spatial distribution of the alteration zones derived from the ASTER data at the regional scale, lithogeochemical data were utilized. These geochemical datasets, collected across the Koldar Massif at a scale of 1:10,000, provided essential baseline information for verifying the presence of ore-related anomalies (Figure 3). A total of 20 elements were analyzed based on a dense sampling grid (100 m × 20 m), among which Cu, Mo, Pb, Zn, Ag, Bi, and W were found to be the most diagnostic for the mineralization processes [2]. The integration of this geochemical map allowed for cross-validation of remote sensing results, enhancing the reliability of the interpreted alteration zones.

This study was conducted following the formulation of a clear problem statement, identification of a knowledge gap, and establishment of the main research objectives. To investigate the hydrothermal alteration minerals associated with porphyry copper mineralization in eastern Kazakhstan, we employed a multi-resolution remote sensing approach using the ASTER and WorldView-3 datasets. These sensors were selected based on their complementary capabilities. The methodological framework consists of three main stages: pre-processing, spectral analysis, and post-processing with validation. In the pre-processing stage, both datasets underwent radiometric and atmospheric correction to ensure consistency and accuracy in the spectral reflectance values. These corrections were essential to minimize the distortions caused by sensor characteristics and atmospheric conditions, thereby enabling reliable spectral interpretation. Following pre-processing, the data were subjected to spectral analysis techniques aimed at identifying key alteration minerals. This included the application of false color composite (FCCs), band ratio (BRs), and the Spectral Angle Mapper (SAM) implemented in ENVI 5.3 software (version 5.3, Harris Geospatial Solutions, Broomfield, CO, USA). The selection of these techniques was

informed by the established remote sensing literature, particularly studies focused on mineral exploration in porphyry copper systems. In the final stage, the detected alteration zones were validated through a comprehensive multi-scale approach. Regional-scale validation was conducted using geological maps and the published mineral occurrence data. Point-based validation involved cross-referencing known mineralized locations and field observations, while local-scale validation utilized high-resolution interpretation of WorldView-3 imagery and, where available, ground truth data. This tiered validation strategy ensured robustness and reliability in the interpretation of remote sensing results. The overall methodology is illustrated in Figure 4, which outlines the sequential steps from data acquisition to validation.

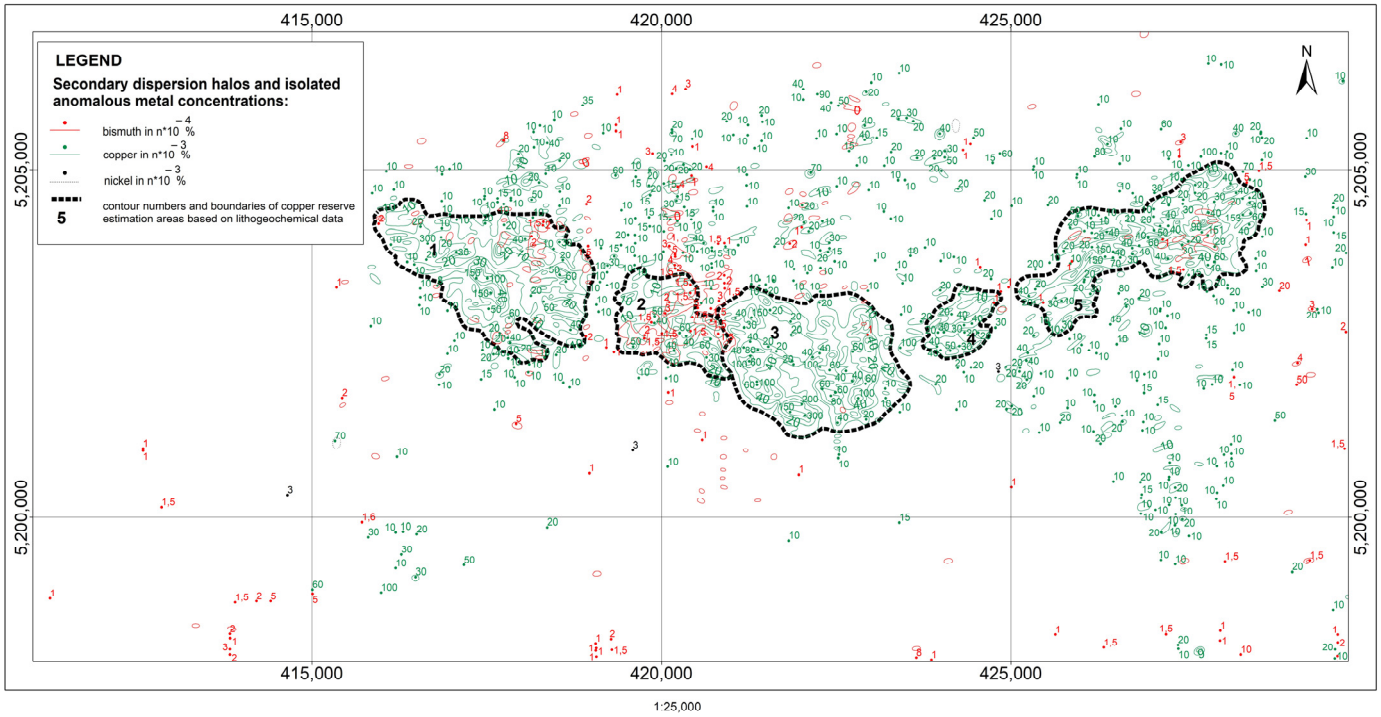


Figure 3. Lithogeochemical map of the Koldar Massif.

3.1. Remote Sensing Data Characteristics

The ASTER multispectral data were used for regional analysis across the Koldar Massif to preliminarily identify the areas potentially associated with mineralization. The ASTER Level 1B data, acquired on 30 May 2004, from the NASA Earthdata platform (https://search.earthdata.nasa.gov, accessed on 5 February 2024), were selected due to their ability to analyze Earth's surface features such as mineralogical composition, temperature anomalies, and hydrothermal zones. The chosen image had minimal cloud cover and sparse vegetation, offering the optimal surface exposure for geological interpretation. Importantly, the image predates mining operations at the deposit, making it appropriate for assessing natural, pre-development conditions. The pre-processing steps included radiometric calibration, FLAASH atmospheric correction, band stacking, and spatial resampling. Vegetation was masked using the Normalized Difference Vegetation Index (NDVI) derived from the ASTER VNIR bands, with a threshold of NDVI > 0.2 applied to exclude vegetated areas.

The ASTER sensor includes 14 spectral bands: 3 in the (VNIR) range with a spatial resolution of 15 m, 6 in the (SWIR) range with a 30 m resolution, and 5 in the (TIR) range with a 90 m resolution. Each ASTER scene covers an area of 60 km × 60 km [41,42]. As previously noted, the SWIR range is critical for detecting the clay and hydroxyl-bearing minerals typical of hydrothermal alteration zones.

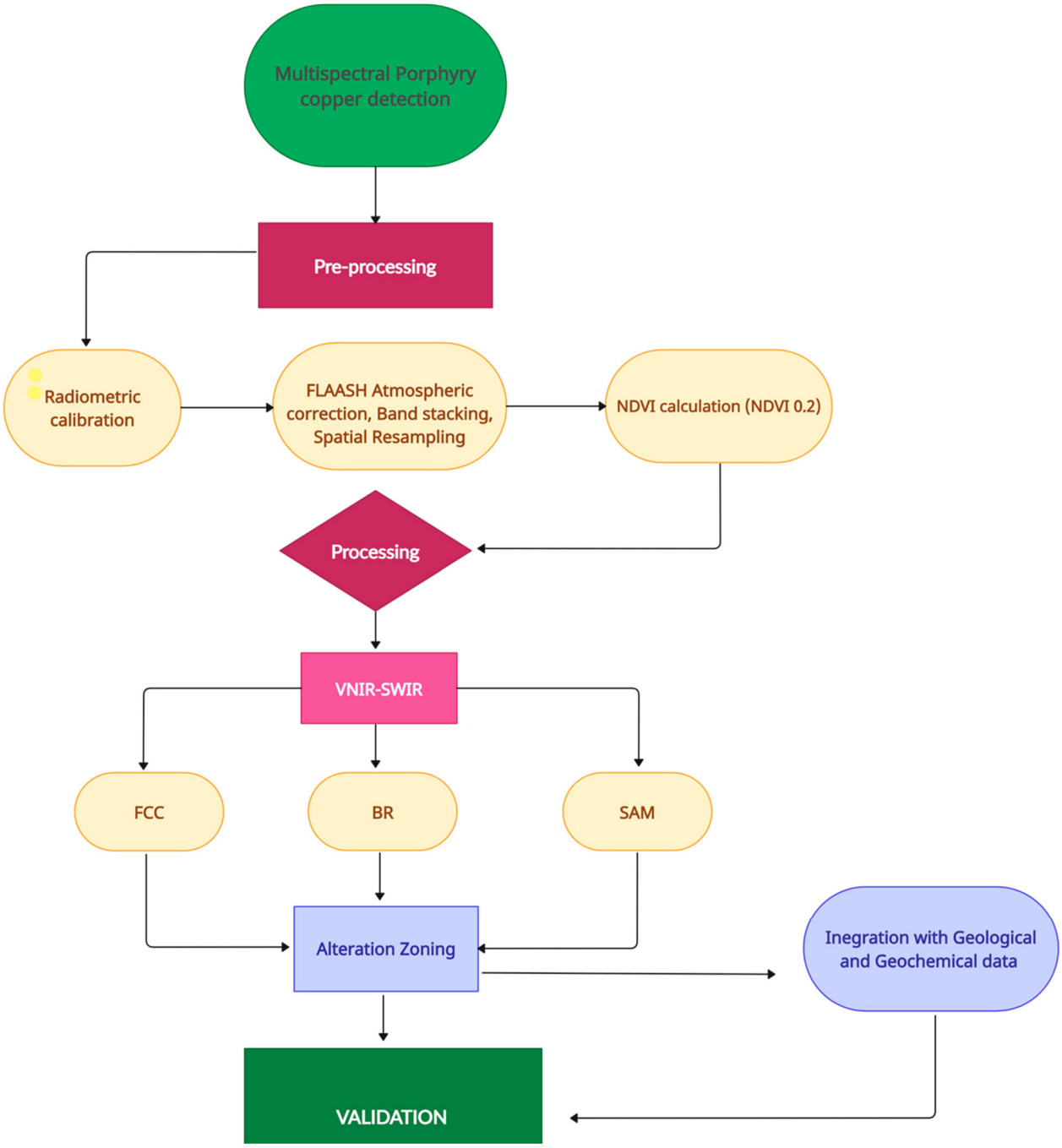


Figure 4. Methodology flowchart of the study.

The WorldView-3 satellite provides high-resolution multispectral imagery and was used for detailed analysis. A cloud-free image acquired on 11 May 2019 covers an area of 25.4 km^2. The spatial resolution of the data is 1.24 m for the VNIR range and 3.7 m for the SWIR range, making it suitable for fine-scale mapping of surface mineralogy. WorldView-3 includes 8 bands in the VNIR range (0.4–1.04 µm) and 8 bands in the SWIR range (1.2–2.5 µm). Although it lacks thermal infrared (TIR) bands, which are particularly sensitive to quartz, feldspar, and some carbonates, the SWIR bands can still detect the characteristic absorption features of hydroxyl-bearing and some carbonate minerals. The higher spatial resolution of WorldView-3 enables more detailed structural and mineralogical mapping compared to ASTER. The acquisition date was selected to reduce vegetation interference during the mineral signature interpretation [37].

ASTER and WorldView-3 sensors are widely employed in geological studies due to their spectral sensitivity, which supports interpretation of mineral composition, structural features, and geomorphological patterns. Spectral bands in the visible, near, and shortwave infrared (SWIR) regions enable identification of geological formations based on their material composition and genesis and secondary alterations related to mineralization processes [35,43]. SWIR bands are especially useful in distinguishing rocks with different mineral compositions and in mapping alteration zones, including the clays and iron oxides associated with porphyry copper deposits [44].

The ASTER data were primarily used for regional analysis and mineralization prediction, while the WorldView-3 data supported detailed mapping of deposits and identification of small-scale geological structures. The combination of ASTER's spectral sensitivity in the SWIR region (TIR bands were not used in this study) and WorldView-3's high spatial resolution provides a powerful multi-scale approach for identifying hydrothermal alteration minerals and geological structures. The detailed sensor specifications are provided in Table 1.

Table 1. Characteristics of the acquired satellite image.

Characteristic	ASTER	WorldView-3
Date of Shooting	30/05/2004	11/05/2019
Spatial Resolution	15 m (VNIR), 30 m (SWIR), 90 m (TIR)	1.24 m (VNIR), 3.7 m (SWIR), 0.31 m (panchromatic)
Spectral Bands	14 (3 VNIR, 6 SWIR, 5 TIR)	16 (8 VNIR, 8 SWIR)
Main Applications	Regional studies, hydrothermal zone mapping, lithological mapping	Detailed mapping, ore zone delineation, structural geology analysis
Mineral Identification Accuracy	Moderate	High
Field of Application	Medium- and large-scale studies	Local and high-detail studies

Hydrothermal alteration associated with Cu–porphyry deposits is typically zoned, forming concentric patterns centered on the intrusion. According to the classic model by Lowell and Guilbert (1970) [45], these zones include the following: (1) a central potassic zone (characterized by secondary biotite and K-feldspar), (2) a surrounding phyllic (sericitic) zone (rich in muscovite, sericite, and quartz), (3) an argillic zone (dominated by kaolinite and smectite), and (4) a peripheral propylitic zone (with chlorite, epidote, and carbonates). Each zone has distinct spectral absorption features that can be detected using multispectral remote sensing.

ASTER's SWIR bands (Bands 4–9, 1.6–2.43 μm) are particularly effective in identifying Al-OH and Mg-OH absorption features in minerals such as muscovite (~2.20 μm), kaolinite (~2.17 and 2.20 μm), and chlorite (~2.25 μm).

WorldView-3 offers 8 SWIR bands (ranging from 1.19 to 2.365 μm, including Band 8: 2.295–2.365 μm) at a 3.7 m spatial resolution and 8 VNIR bands at 1.24 m. This spectral range allows the detection of key alteration minerals, including carbonates, which show absorption features between 2.305 and 2.345 μm (e.g., magnesite and siderite). The high spatial resolution of WorldView-3 makes it particularly useful for detailed lithological and mineralogical mapping, especially in structurally complex terrains. To support the interpretation of remotely sensed data, representative reflectance spectra of key alteration minerals were obtained from the USGS spectral library. These include the minerals commonly associated with phyllic (muscovite, quartz, and pyrite), argillic (kaolinite, montmorillonite, and illite), and propylitic (calcite, chlorite, and epidote) zones (Figure 5). These spectra serve as a reference for understanding the spectral behavior characteristic of each hydrothermal alteration type.

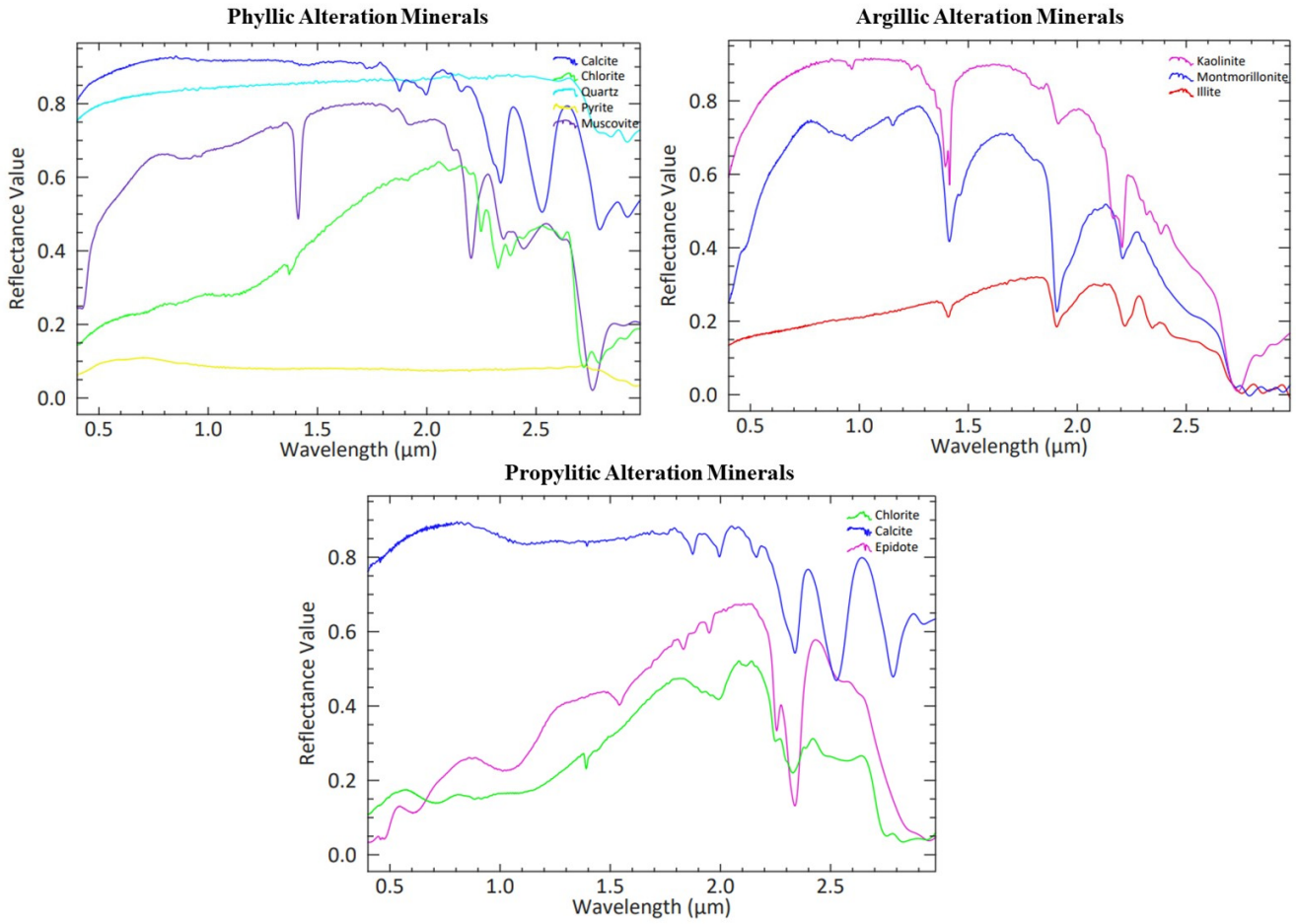


Figure 5. Spectral signatures of alteration minerals associated with phyllic, argillic, and propylitic zones in porphyry copper systems.

3.2. Remote Sensing Techniques

3.2.1. False Color Composites (FCCs)

In remote sensing, false color composites (FCCs) are a widely used visualization method that enhances geological features by reassigning spectral bands to the red, green, and blue (RGB) channels based on their diagnostic spectral properties [46]. Unlike true color imagery, FCC utilizes spectral ranges such as (NIR) and (SWIR) to emphasize compositional variations in surface materials. Specific band combinations are chosen according to the analysis goals and the spectral behavior of target minerals, particularly those related to hydrothermal alteration processes [47].

In this study, false color composites (FCCs) were generated using band combinations adopted from previously published research. For the ASTER data, the RGB combination of R = Band 4 (1.65–1.75 μm), G = Band 6 (2.185–2.225 μm), and B = Band 8 (2.295–2.365 μm) was used, which has been shown to effectively enhance hydrothermal alteration features in similar geological settings [35]. For the WorldView-3 imagery, the RGB combination of R = Band 3 (Red Edge), G = Band 6 (NIR1), and B = Band 8 (SWIR1) was applied, following recommendations from prior studies focused on high-resolution mineral mapping [35,48,49].

The geological rationale behind these combinations is as follows:

These combinations were selected based on the known spectral behavior of the hydrothermal alteration minerals present in the Koldar Massif. ASTER Band 4 is sensitive to ferric iron, helping to detect the oxidized zones. Band 6 responds to the Al–OH absorption features typical for muscovite and kaolinite (phyllic and argillic alterations), while Band 8 is useful for identifying Mg–OH-bearing minerals such as chlorite and epidote (propylitic alteration).

In WorldView-3, the combination enhances shortwave and near-infrared responses from altered clays, aiding in the differentiation of lithological units within the massif [48–50].

The FCC images served as an effective visual tool for the preliminary identification of hydrothermal alteration zones across the Koldar Massif. Color anomalies, particularly reddish and greenish tones, helped emphasize areas likely enriched in hydroxyl-bearing minerals. These visually distinct zones generally corresponded to copper occurrences of various formations and were subsequently cross-checked using spectral ratio techniques and partially verified during fieldwork. Thus, FCC analysis played a crucial role in the initial narrowing down of prospective targets for more detailed investigation.

3.2.2. Band Ratios

Band ratios are a commonly applied technique in remote sensing that enhance feature contrast by dividing the spectral values of one band by another. This method helps in highlighting hydrothermal alteration minerals such as chlorite and quartz, while reducing the impact of topographic effects by normalizing differences between shaded and illuminated surfaces. It facilitates differentiation of lithological units, structural features, and mineral alteration zones, especially in areas where features are not distinguishable in raw spectral bands. However, false anomalies may arise in regions with dense vegetation or anthropogenic modifications, necessitating further analysis [3,13,51–53].

Band ratios are widely used in remote sensing for highlighting the spectral features associated with hydrothermal alteration minerals. For instance:

- (2/1) and (4/2): to highlight ferric iron oxides.
- (5/6) and (6/8): for detecting Al-OH- and Mg-OH-bearing minerals (e.g., kaolinite, muscovite, chlorite, and epidote).
- (7/6): sensitive to Al-OH absorption near 2.2 μm.
- (8/9): useful for detecting Mg-OH absorption [4,11].

In this study, a composite image using the band ratios 5/6 (Red), 9/8 (Green), and 7/6 (Blue) was generated to enhance and differentiate the key hydrothermal alteration zones within the study area. This combination was selected based on its proven ability to effectively distinguish between argillic, propylitic, and phyllic alteration types, as supported by previous studies [4,11].

- The 5/6 ratio is particularly effective in highlighting argillic alteration, as it enhances the spectral response of clay minerals such as kaolinite and illite.
- The 9/8 ratio is sensitive to Mg–OH-bearing minerals, commonly associated with propylitic alteration, including chlorite and epidote.
- The 7/6 ratio emphasizes the absorption features of Al–OH-bearing minerals such as muscovite, which are indicative of the phyllic alteration zone [54].

The alteration minerals targeted in this study included the following:

Phyllic alteration includes muscovite, sericite, and quartz. Muscovite and sericite also have Al–OH absorption near 2.20 μm, making them detectable with the same band ratios as argillic minerals. Quartz lacks strong absorption in SWIR but is identified through its association with sericite and muscovite.

Argillic alteration is characterized by the presence of kaolinite, illite, and montmorillonite, which show strong absorption features near 2.17–2.22 μm due to Al–OH bonds. These minerals were detected using ratios like ASTER 5/6 and WorldView-3 SWIR5/SWIR6, which are sensitive to absorption at ~2.2 μm.

Propylitic alteration is marked by chlorite and epidote, which show absorption features around 2.25–2.35 μm linked to Mg–OH and Fe–OH bonds. Band ratios like ASTER 8/9 and WorldView-3 SWIR7/SWIR8 were used to enhance their detection in the peripheral zones.

3.2.3. Spectral Angle Mapper (SAM)

The Spectral Angle Mapper (SAM) is a widely used image classification algorithm that calculates the angle between the spectral vector of an image pixel and a reference spectrum from a laboratory library. Spectra are represented as vectors in an n-dimensional space, where n corresponds to the number of spectral bands. The classification is based on spectral similarity, determined by the direction of the vectors rather than their magnitude. A smaller angle (between 0 and 1) indicates higher similarity, enabling reliable identification of surface materials. The SAM classification in this study followed the approach described by [55] using Formula (1). The method was first introduced by Kruse et al. (1993), who demonstrated its effectiveness for mapping mineralogy from AVIRIS hyperspectral data [55]. The SAM has since become one of the standard tools in spectral analysis for geologic applications [55].

$$\alpha = \cos^{-1}\left[\frac{\sum_{i=1}^{nb} x_i r_i}{\left(\sum_{i=1}^{nb} x_i^2\right)^{\frac{1}{2}}\left(\sum_{i=1}^{nb} r_i^2\right)^{\frac{1}{2}}}\right] \quad (1)$$

This method has been extensively applied in geology and mineral exploration [56–58].

While the SAM is traditionally developed for hyperspectral datasets, several studies have demonstrated its cautious application to multispectral sensors such as ASTER and WorldView-3, particularly when combined with other techniques like band ratios and FCCs [59]. In this study, the SAM was employed not as a standalone classifier but as a complementary tool, calibrated using field observations and results from the BR and FCC methods. This integrative approach helped reduce subjectivity and enhance the interpretability of alteration zone boundaries.

4. Results

4.1. Mapping Alteration Zones and Minerals

4.1.1. FCC

Experimental studies have shown that the color combination RGB = 468 is the most effective for identifying the hydrothermal alteration zones in porphyry copper deposits [60]. Depending on the type of ore deposit, the presence of alteration zones can indicate potential resources in the region. For example, the presence of chlorite is significant for this type of deposit, as it is a common mineral in the outer propylitic alteration zone of porphyry copper systems, indicating low-temperature hydrothermal activity [2,61]. In the given image, the areas with propylitic alterations are marked in green, while the areas with phyllic alteration appear pinkish-yellow (Figure 6). This is explained by the high reflectance of alunite, kaolinite, and muscovite in Band 4 compared to Bands 6 and 8 [62,63]. The resulting map was overlaid with contours from the lithogeochemical map (Figure 3), reflecting stable and local copper anomalies. The spatial coincidence of the spectral features of alterations with geochemical anomalies was recorded.

The WorldView-3 satellite data provided even more detailed results for the Aidarly and Kyzylkiya deposits (Figure 7). Unlike ASTER, the WorldView-3 images are characterized by a higher spatial resolution, enabling more precise mapping of small-scale geological structures and mineralogical changes within these deposits. This improvement in detail makes WorldView-3 the preferred tool for local investigational studies of specific areas requiring high accuracy (Figure 7).

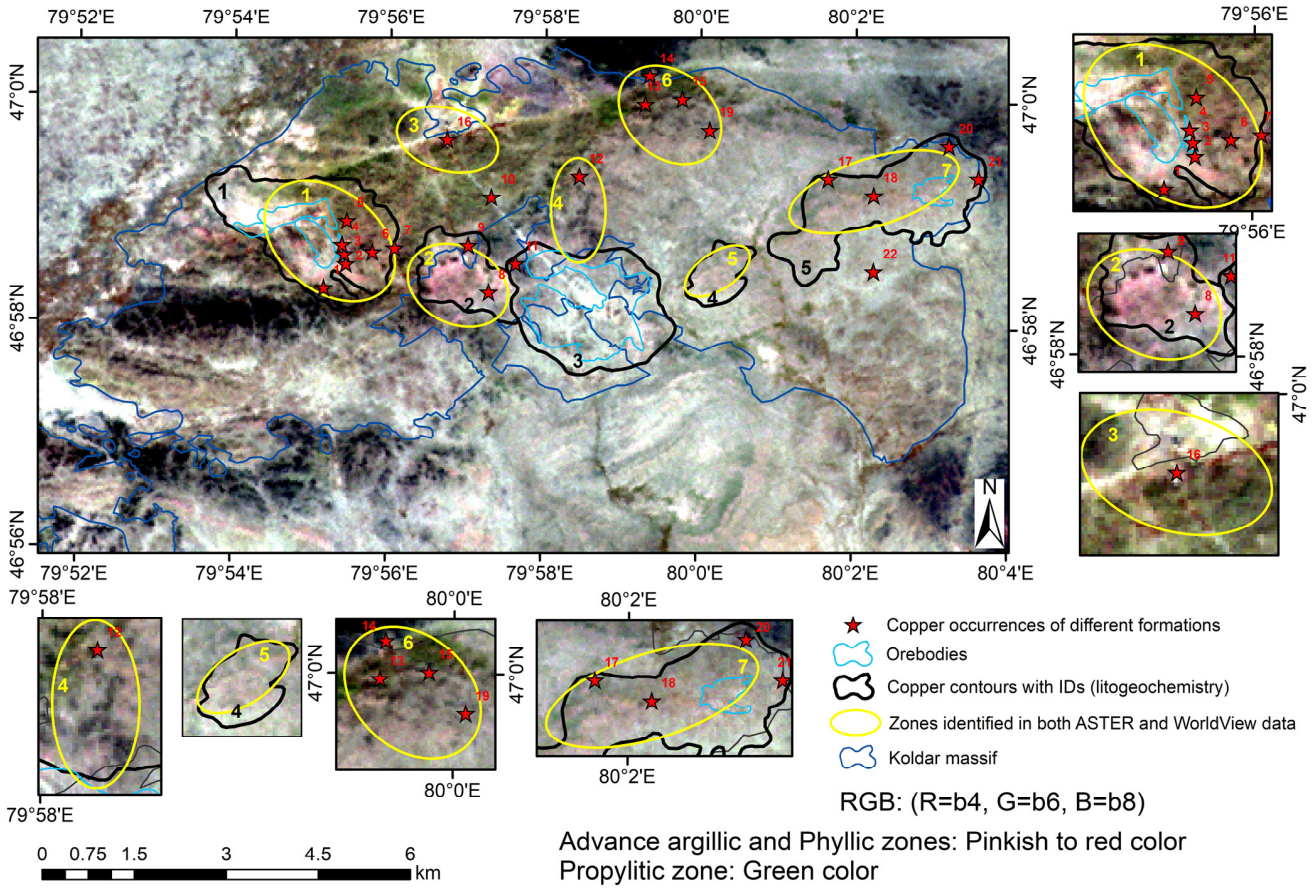


Figure 6. Demonstration of ASTER data processing to identify areas rich in kaolinite and muscovite. False color composite in RGB mode (R = 4, G = 6, B = 8). Green color indicates propylitic alterations, while pinkish-yellow color represents areas of argillic alteration.

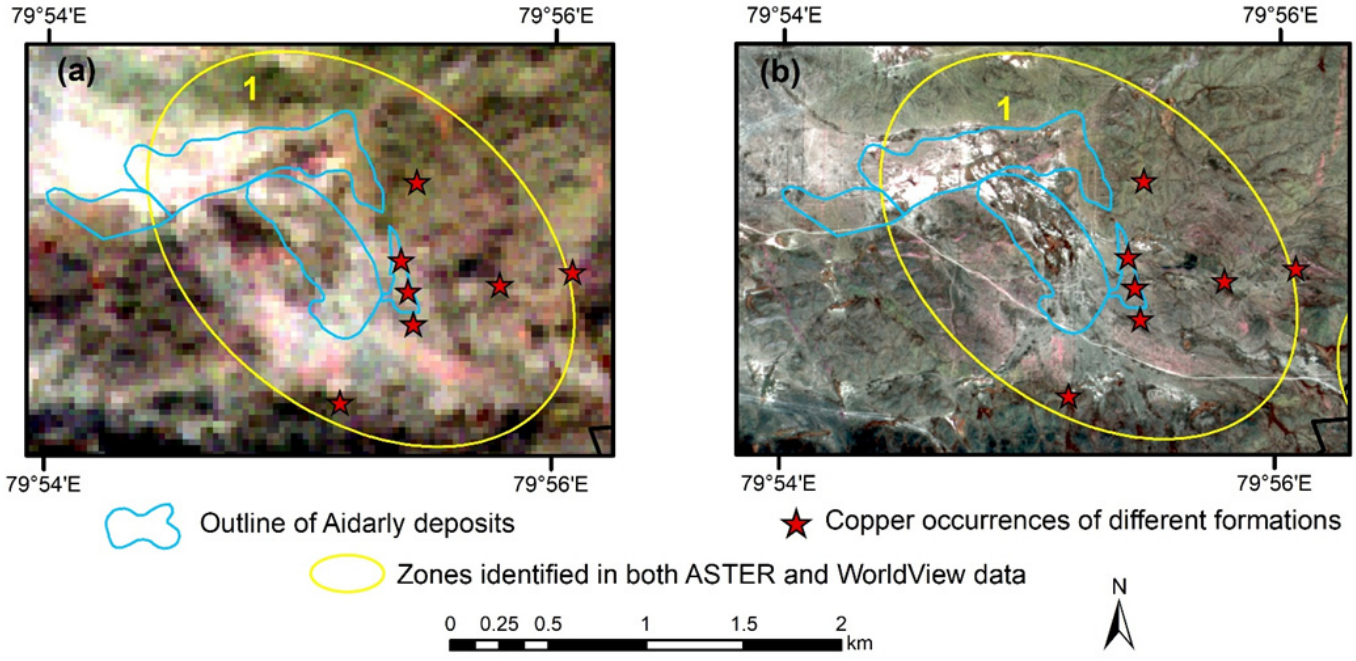


Figure 7. Demonstration of ASTER and World View-3 data processing to identify kaolinite and muscovite-rich areas. (**a**) False color composite in RGB mode (R = 4, G = 6, B = 8). Green indicates propylitic alteration, and pinkish-yellow represents phyllic alteration areas. (**b**) False color composite in RGB mode (R = 3, G = 6, B = 8). Green indicates propylitic alteration, and pinkish-yellow represents phyllic alteration areas.

We compared the hydrothermal alteration zones derived from ASTER Figure 7a and WorldView-3 Figure 7b using RGB false color composites (7/6, 5/6, 8/9). While both sensors delineate similar zones, WorldView-3 provides sharper boundary definitions and higher positional accuracy due to its finer spatial resolution (3.7 m vs. 30 m in SWIR), reducing spectral mixing and improving detection of small-scale alteration features, as also confirmed by [35].

In particular, features that appear blurred or overgeneralized in ASTER due to pixel mixing are more discretely resolved in WorldView-3, especially along the flanks of the alteration zones and within narrow structural corridors.

4.1.2. BR

Taking into account the spectral specifications of the target minerals, particularly within the Koldar Massif, band ratio (BR) combinations were applied to determine the spatial distribution of the hydrothermal alteration zones enriched with iron oxides and clay minerals. The ASTER Level 1B dataset used for this analysis was acquired on 30 May 2004 from the NASA Earthdata platform (cloud-free and minimal vegetation). Before the band ratio processing, the data underwent radiometric calibration, atmospheric correction, band stacking, and resampling to ensure consistency. To map the phyllic, argillic, and propylitic zones in the study area, an RGB composite using band ratios 7/6, 5/6, and 8/9 (R: 7/6, G: 5/6, B: 8/9) was developed based on the established practices in hydrothermal alteration mapping with ASTER data used by [11,64,65].

The 5/6 and 8/9 ratios on ASTER are sensitive to minerals with Al–Si–OH absorption (kaolinite and muscovite/sericite) and Mg–Si–OH absorption (chlorite and epidote), respectively; the 7/6 ratio targets muscovite-rich zones associated with phyllic alteration. Band ratios such as 5/6 (Al-OH) and 8/9 (Fe–Mg-OH/carbonate) on ASTER are widely recommended in the literature for detecting argillic and propylitic alterations [64–68]. The phyllic alteration zone appears as yellow/reddish-yellow, the argillic in green, and the propylitic in blue shading (Figure 8).

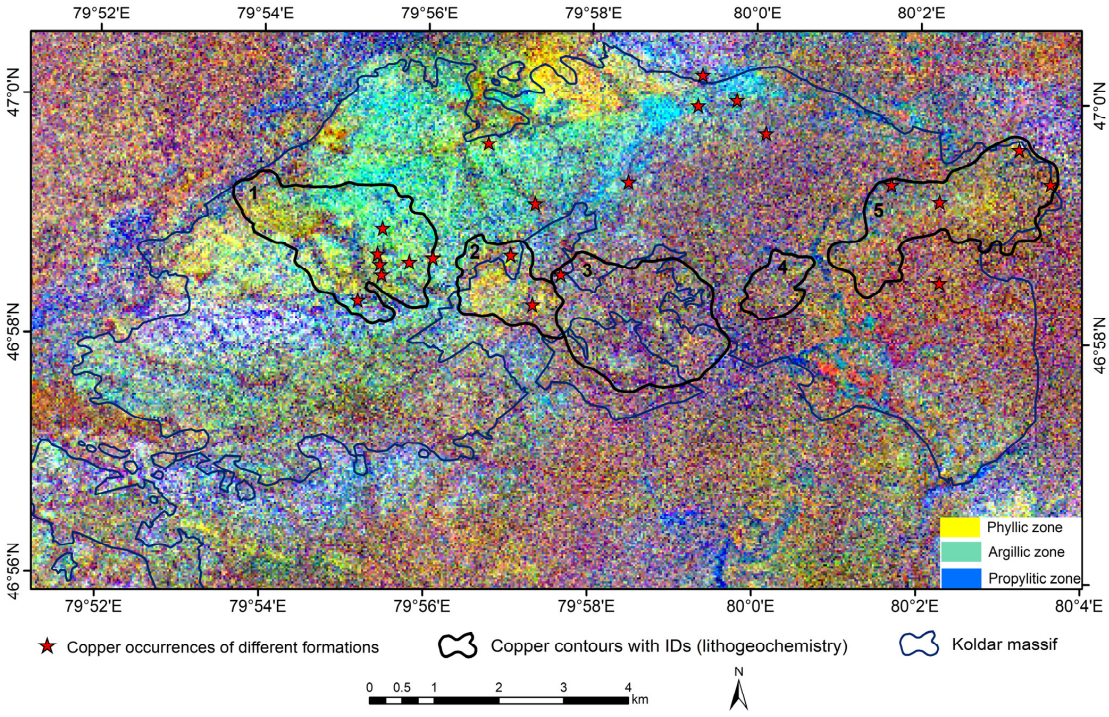


Figure 8. Resulting image for contrast zones. Band ratios 5/6, 9/8, and 7/6 as RGB composite colors obtained from ASTER data: phyllic zone—yellow or reddish-yellow; argillic zone—green; and propylitic zone—blue.

4.1.3. SAM

The Spectral Angle Mapper (SAM) method was applied on ASTER and WorldView-3 to delineate the hydrothermally altered zones in the study area (Figure 9). As a result of the analysis, propylitic, argillic, and phyllic alterations were successfully identified, indicating the presence of potentially productive mineralization zones. Propylitic alterations are characterized by significant chlorite and epidote minerals, which may indicate low-temperature metamorphic processes. Argillic alterations are associated with clay minerals such as kaolinite and montmorillonite, pointing to intense hydrothermal fluid activity. Phyllic alterations, represented by finely layered metamorphic rocks, contain sericite and quartz, further confirming the presence of hydrothermal activity. This data enables more precise localization of mineralization zones for further detailed investigations.

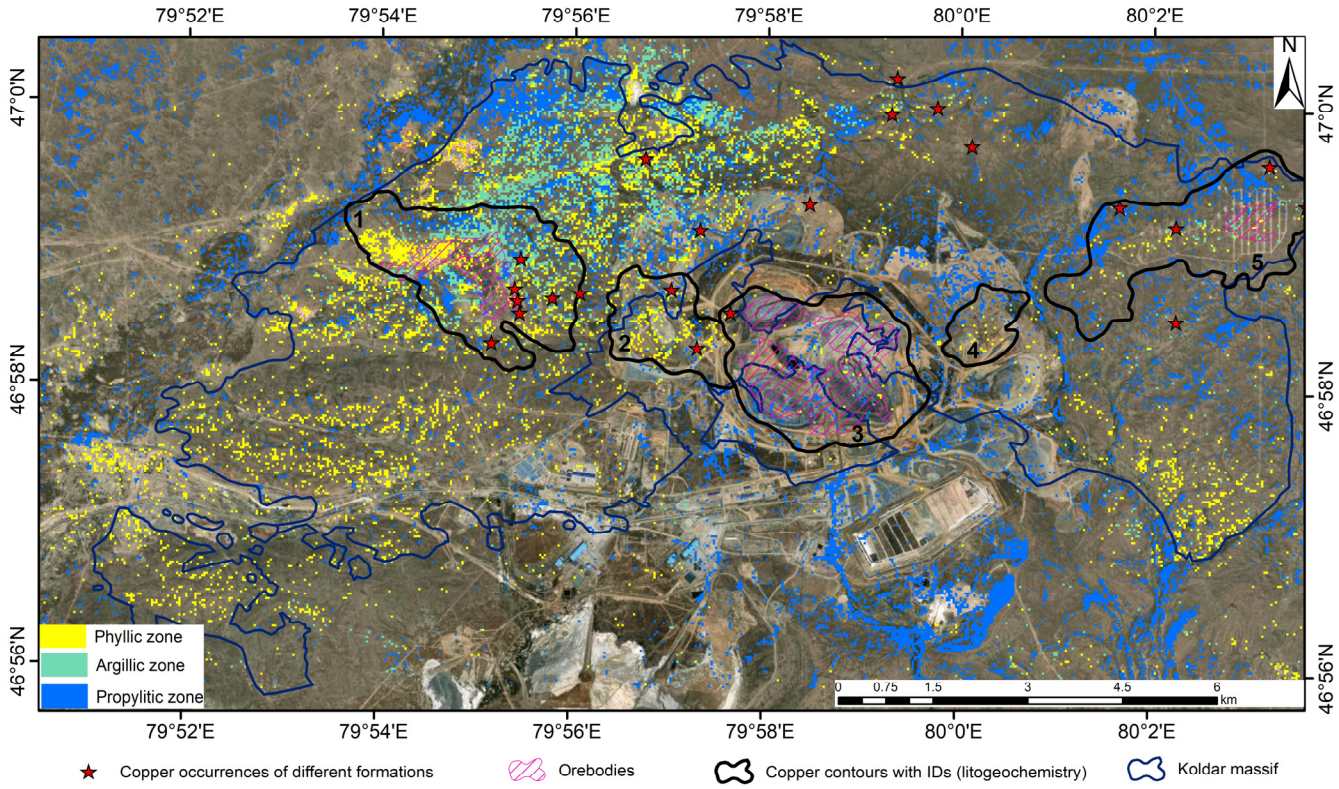


Figure 9. Delineation of hydrothermally altered zones using the SAM method on ASTER data.

The zones of phyllic, argillic, and propylitic alterations were mapped using the SAM algorithm applied to the ASTER and World View-3 images (Figure 9). The reference spectra were selected from the USGS Digital Spectral Library to support the spectral analysis and classification of hydrothermal alteration minerals. The spectral angles (in radians) used in this study were as follows: $\alpha = 0.08$ for the phyllic alterations, $\alpha = 0.065$ for the argillic alterations, and $\alpha = 0.07$ for the propylitic alterations. The results of the SAM classification based on ASTER are presented in Figure 9. The contours constructed using the lithochemical map data (Figure 3) were superimposed on the resulting spectral classification map. As a result, a spatial correspondence was recorded between the phyllic alteration zones and areas with stable and local anomalies in copper content.

Figure 10 presents the SAM classification results from the ASTER (Figure 10a) and WorldView-3 (Figure 10b) data. The ASTER-derived map shows broader alteration zones extending beyond the Aidarly deposit, partly due to its lower spatial resolution (30 m), which causes pixel mixing and generalization. In contrast, the WorldView-3 classification, with its finer 3.7 m SWIR resolution, highlights more compact and spatially precise phyllic and argillic zones that correlate well with the deposit contours and copper anomalies.

These observations support the value of a multi-scale remote sensing strategy: ASTER effectively highlights regional alteration trends and potential targets, while WorldView-3 refines these targets, improves spatial accuracy, and reduces the false positives arising from coarse pixel blending.

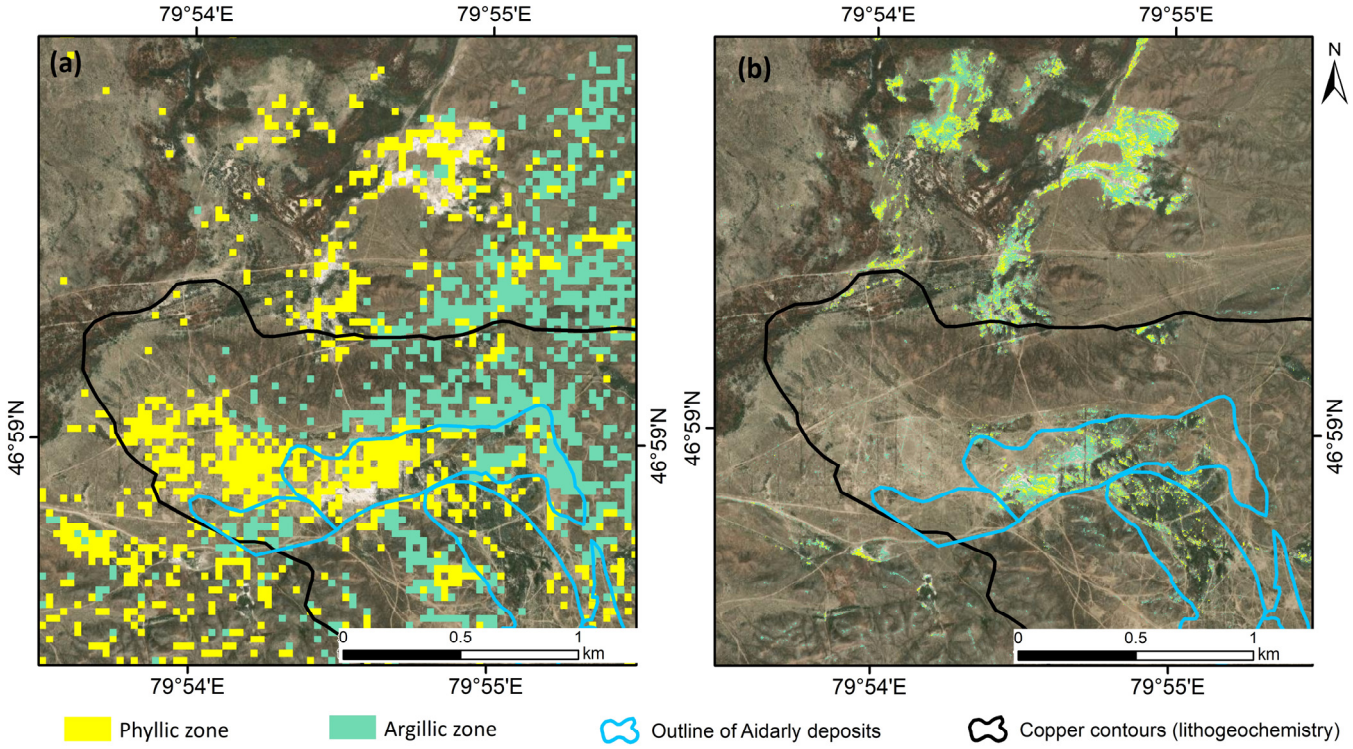


Figure 10. A comparison of the SAM results with the geological map of the study area: (**a**) identified altered zones based on ASTER data, and (**b**) identified altered zones based on WorldView-3 data.

As a result of processing the WorldView-3 multispectral data at the Aidarly deposit, distinct and consistent zones of hydrothermally altered minerals were identified. These zones show a strong correlation with the ore zones of this deposit and with the delineated deposit boundaries. Furthermore, a similar hydrothermally altered zone was discovered north of Aidarly (Figure 11a), exhibiting characteristics comparable to those of the Aidarly deposit.

This newly identified prospective structure requires further investigation to assess its potential. Including this zone as a target for detailed study opens new opportunities for expanding exploration activities in the Aidarly area, potentially leading to the discovery of additional resources (Figure 11).

In addition, such systems are characterized by the typical porphyry zoning of alterations, including the phyllitization and argillitization zones, successively changing from the center to the periphery. Phyllitic alterations are directly related to high-quality copper mineralization: the more clearly expressed and ordered the zoning, the higher the copper content in the mineralization. Therefore, the spatial patterns of the distribution of phyllitization zones are an important feature in the search for mineral deposits [15].

4.2. Verification of Remote Sensing Results

Three primary hydrothermal alteration zones—phyllic, argillic, and propylitic—were successfully mapped in the Koldar region using band ratio (BR), false color composite (FCC), and Spectral Angle Mapper (SAM) techniques applied to ASTER data (Figures 6, 7 and 9). The identified alteration zones are predominantly concentrated in the northern and northwestern parts of the Koldar Massif. For a more detailed analysis and validation, the Aidarly

deposit was selected as a representative site due to its clear expression of these alteration features. For this purpose, a commercial WorldView-3 image was acquired

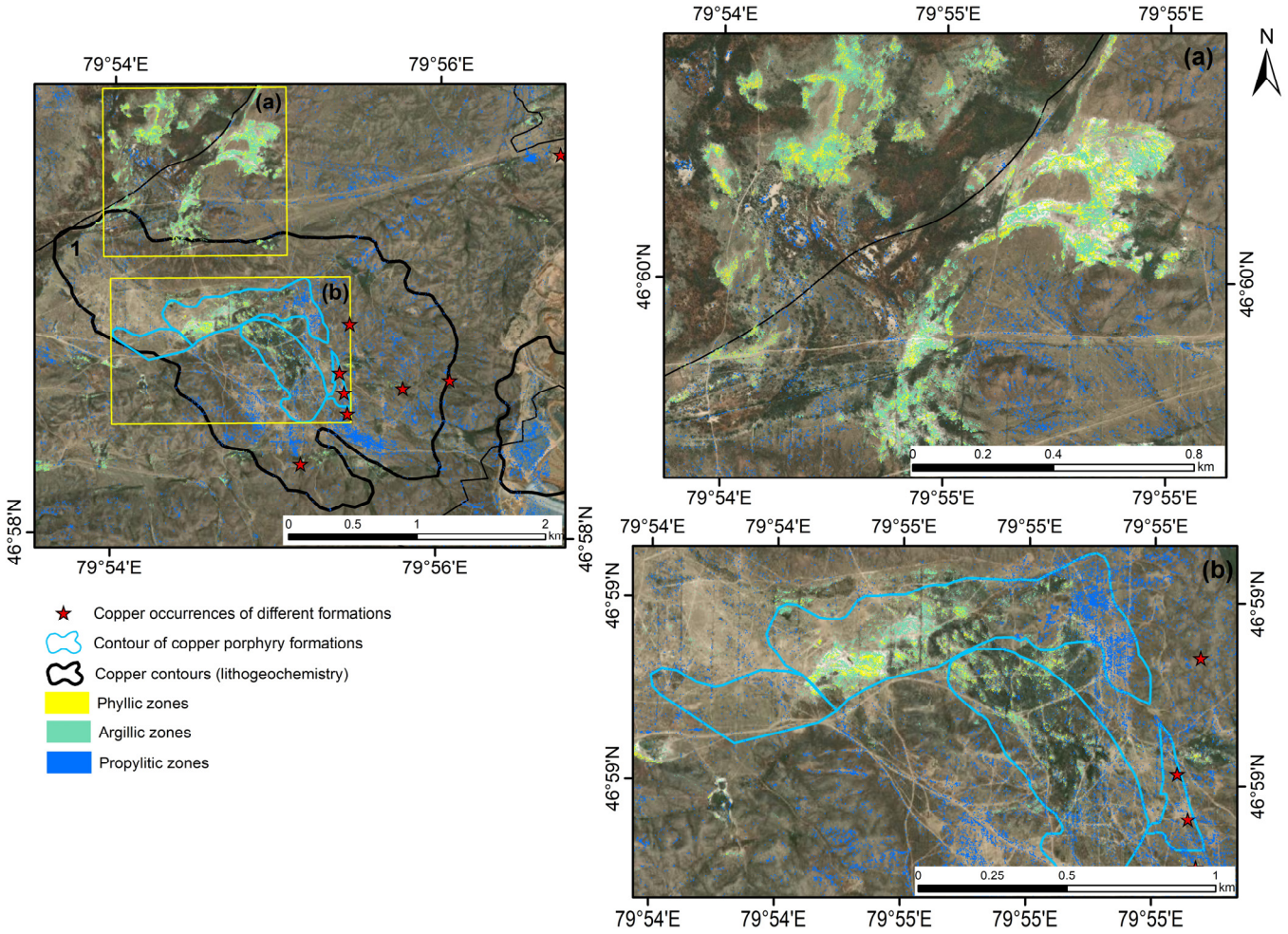


Figure 11. Detailed spectral mapping using the SAM method on WorldView-3 data, highlighting argillic (green) and phyllic (red) alterations: (**a**)—new prospective area, and (**b**)—Aidarly deposit.

A clear spatial correlation between the distribution of hydrothermal alteration zones and lineament density was also observed. As shown in Figure 12, areas with a high concentration of detected lineaments coincide with the previously identified alteration zones in the northwestern part of the Koldar Massif. The spatial distribution, density, and orientation of the lineaments suggest a likely genetic relationship between the hydrothermal alteration zones and the underlying copper porphyry mineralization.

In Figure 12, the distribution of pixels classified as phyllic and argillic alteration zones (based on the SAM method using ASTER data) is overlaid on the lineament density map. Although the precise boundaries of these zones could not be delineated, the occurrence pattern of the classified pixels correlates well with the results of the BR, FCC, and the identified lineament structures, supporting the interpreted alteration zonality.

To ensure the reliability of the identified hydrothermal alteration zones, a three-tiered validation approach was implemented, incorporating regional, point-based, and local-scale assessments using independent geological and geochemical data sources.

4.2.1. Regional-Scale Validation Using Lithochemical Data

To assess the geological validity of the alteration zones identified using the ASTER data (Figures 6, 8 and 9), a regional-scale comparison was conducted using a lithogeochemical

map (Figure 3) containing five dispersion contours based on stable copper anomalies and isolated high-value points. The highest correspondence with the ASTER-interpreted alteration zones was observed in the first and second contours, located in the western part of the massif. Notably, the first contour includes the Aidarly deposit, where all three methods—band ratio (Figure 6), false color composite (Figure 7), and the Spectral Angle Mapper (Figure 9)—consistently delineated phyllic and argillic alteration zones. The second contour, situated between the Aidarly and Aktogay deposits, also demonstrated strong alignment with phyllic alteration features.

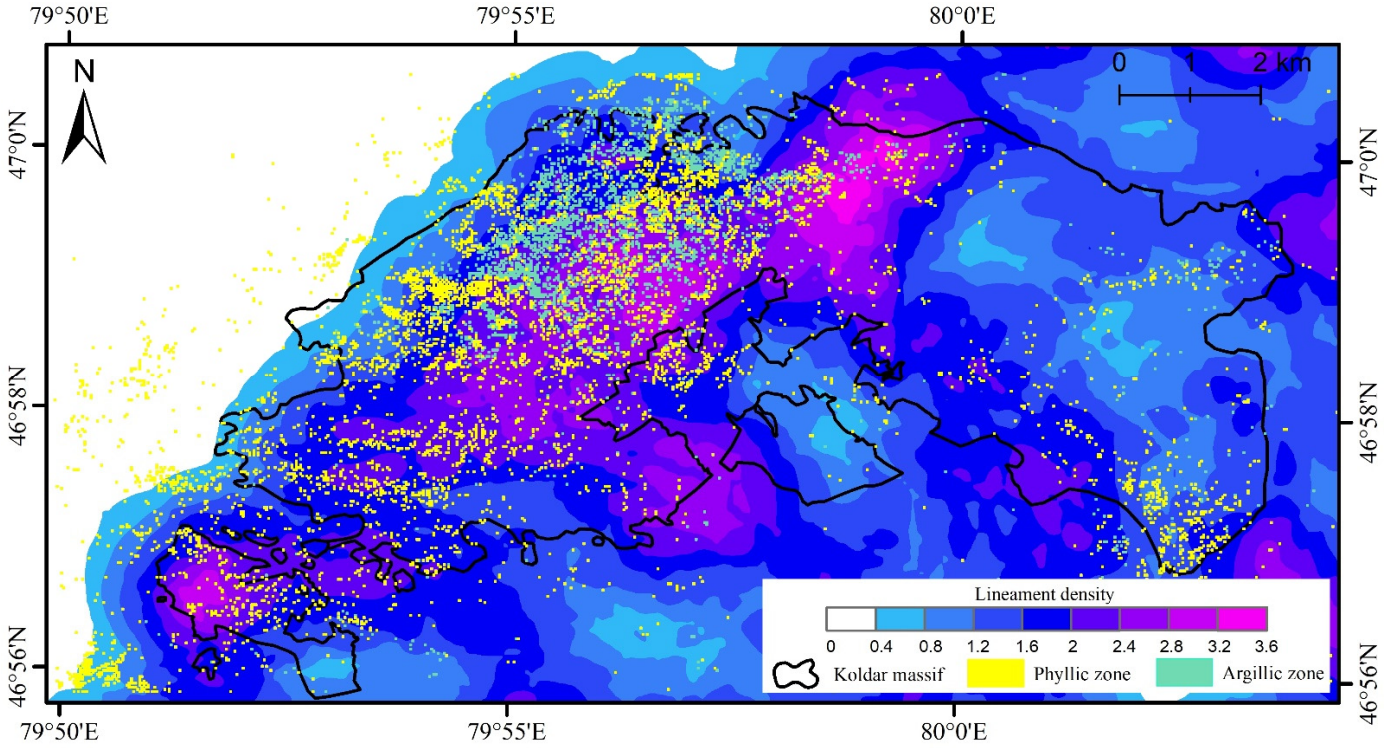


Figure 12. Spatial distribution of lineament density derived from the Digital Elevation Model (DEM) using the LINE module in PCI Geomatica across the study area. The image also includes an overlay of SAM-derived phyllic and argillic alteration pixels to illustrate their spatial relationship with lineament structures.

The third contour, encompassing the Aktogay deposit, showed weak spectral signatures of argillic and phyllic alterations, but the presence of propylitic alteration was prominent, which is consistent with the volcanic rock cover observed during the satellite acquisition period. The fourth and fifth contours, covering the areas between Aktogay and Kyzylkiya and the Kyzylkiya deposit itself, respectively, displayed moderate agreement with the ASTER-derived alteration zones. Here, the detected pixels of phyllic alteration partially coincided with known copper occurrences.

This regional validation confirms that the hydrothermal alteration zones mapped from the ASTER data are geologically meaningful and spatially consistent with lithochemical anomalies.

4.2.2. Point-Based Accuracy Assessment Using Known Copper Occurrences

To quantitatively assess the accuracy of the ASTER-based interpretation, 22 reference points corresponding to known copper occurrences from various geological formations (based on the works of Krasnikov A.M. and Belykh P.) were used (Table 2). These points were compared with the phyllic alteration zones delineated by the band ratio (BR) (Figure 6), false color composite (FCC) (Figure 7), and Spectral Angle Mapper (SAM) (Figure 9)

methods. Phyllic alteration was selected as the primary focus for validation due to its strong spatial correlation with, and indicative value for, copper mineralization in the study area. In porphyry copper systems, phyllic zones—characterized by minerals such as sericite, illite, and quartz—commonly occur closer to ore-bearing bodies and are often formed by the intense hydrothermal activity associated with copper deposition [1]. This makes them a more geologically meaningful target for validation compared to argillic or propylitic alterations.

Table 2. Copper occurrence points from various formations based on the geological map of the Koldar Massif (following A.M. Krasnikov).

Sample No	Longitude	Latitude	BR	FCC	SAM
1	79°55′10.006″ E	46°58′18.144″ N	Yes	Yes	No
2	79°55′27.126″ E	46°58′31.031″ N	Yes	Yes	Yes
3	79°55′25.808″ E	46°58′36.275″ N	Yes	Yes	Yes
4	79°55′24.023″ E	46°58′41.290″ N	Yes	Yes	Yes
5	79°55′27.525″ E	46°58′54.009″ N	Yes	No	Yes
6	79°55′47.392″ E	46°58′37.567″ N	Yes	Yes	Yes
7	79°56′4.630″ E	46°58′39.785″ N	Yes	Yes	Yes
8	79°57′17.712″ E	46°58′16.972″ N	Yes	Yes	Yes
9	79°57′1.450″ E	46°58′41.681″ N	Yes	Yes	Yes
10	79°57′18.984″ E	46°59′7.384″ N	No	No	Yes
11	79°57′38.202″ E	46°58′32.245″ N	No	No	Yes
12	79°58′26.887″ E	46°59′18.959″ N	No	Yes	Yes
13	79°59′17.199″ E	46°59′57.764″ N	No	Yes	Yes
14	79°59′20.357″ E	47°0′13.006″ N	No	Yes	No
15	79°59′45.649″ E	47°0′0.586″ N	No	Yes	Yes
16	79°56′44.433″ E	46°59′37.528″ N	Yes	Yes	Yes
17	80°1′39.411″ E	46°59′19.139″ N	Yes	Yes	Yes
18	80°2′14.637″ E	46°59′10.651″ N	Yes	Yes	Yes
19	80°0′7.189″ E	46°59′44.274″ N	Yes	Yes	Yes
20	80°3′12.411″ E	46°59′37.275″ N	Yes	Yes	Yes
21	80°3′35.574″ E	46°59′20.109″ N	Yes	Yes	Yes
22	80°2′15.047″ E	46°58′30.368″ N	Yes	No	No
Total number of matched samples			16	18	19
Total number of unmatched samples			6	4	3
Overall accuracy			72.7%	81.8%	86.4%
Kappa coefficient			0.45	0.64	0.73

The results of the matches were as follows:

- The band ratio method provided a match in 16 out of 22 points, corresponding to an accuracy of 72.7%. The calculated kappa coefficient was 0.45, indicating moderate agreement.
- The FCC method detected phyllite changes in 18 out of 22 points, with an accuracy of 81.8% and a kappa coefficient of 0.64, indicating substantial (good) agreement.
- The SAM method showed the best result: the coincidence of change zones was observed in 19 out of 22 points (with an accuracy of 86.4%), with a kappa coefficient of 0.73, indicating a high degree of agreement.

The overall accuracy for all the types of hydrothermal alterations, averaged across the three applied methods (the band ratio, FCC, and SAM), was approximately 0.61, with a corresponding Kappa coefficient of around 0.57. This indicates a moderate level of agreement and reliability across the classification approaches, with the SAM method yielding the highest individual accuracy.

4.2.3. Local-Scale Validation Using WorldView-3 and Geological Map of Aidarly

To perform a high-resolution validation, the Aidarly deposit area was selected for detailed comparison due to its well-defined hydrothermal alteration features in the ASTER data (Figures 6, 7 and 9). WorldView-3 imagery, with a spatial resolution of 3.7 m, was used to analyze the zonal structure of alteration in greater detail.

High-resolution WorldView-3 data confirmed the zoning pattern derived from the ASTER imagery, showing a transition from phyllic to argillic alteration, typical of porphyry copper systems. A new prospective area was also identified north of the Aidarly deposit, exhibiting similar spectral characteristics (Figure 11). While ASTER provided broader coverage and higher sensitivity to subtle spectral changes, its lower resolution led to mixed pixels that may have combined multiple alteration types (Figure 10a). In contrast, WorldView-3 allowed for more precise delineation of the alteration boundaries (Figure 10b).

For a further accuracy assessment, the spatial distribution of the alteration zones interpreted from the WorldView-3 imagery was compared with the detailed geological map of the Aidarly deposit (Figure 2). A strong spatial correlation was observed between the remotely sensed alteration zones and the delineated ore zone obtained from the geological map (Figure 13). This confirms the accuracy of the applied remote sensing methods and supports their integration into mineral exploration practices.

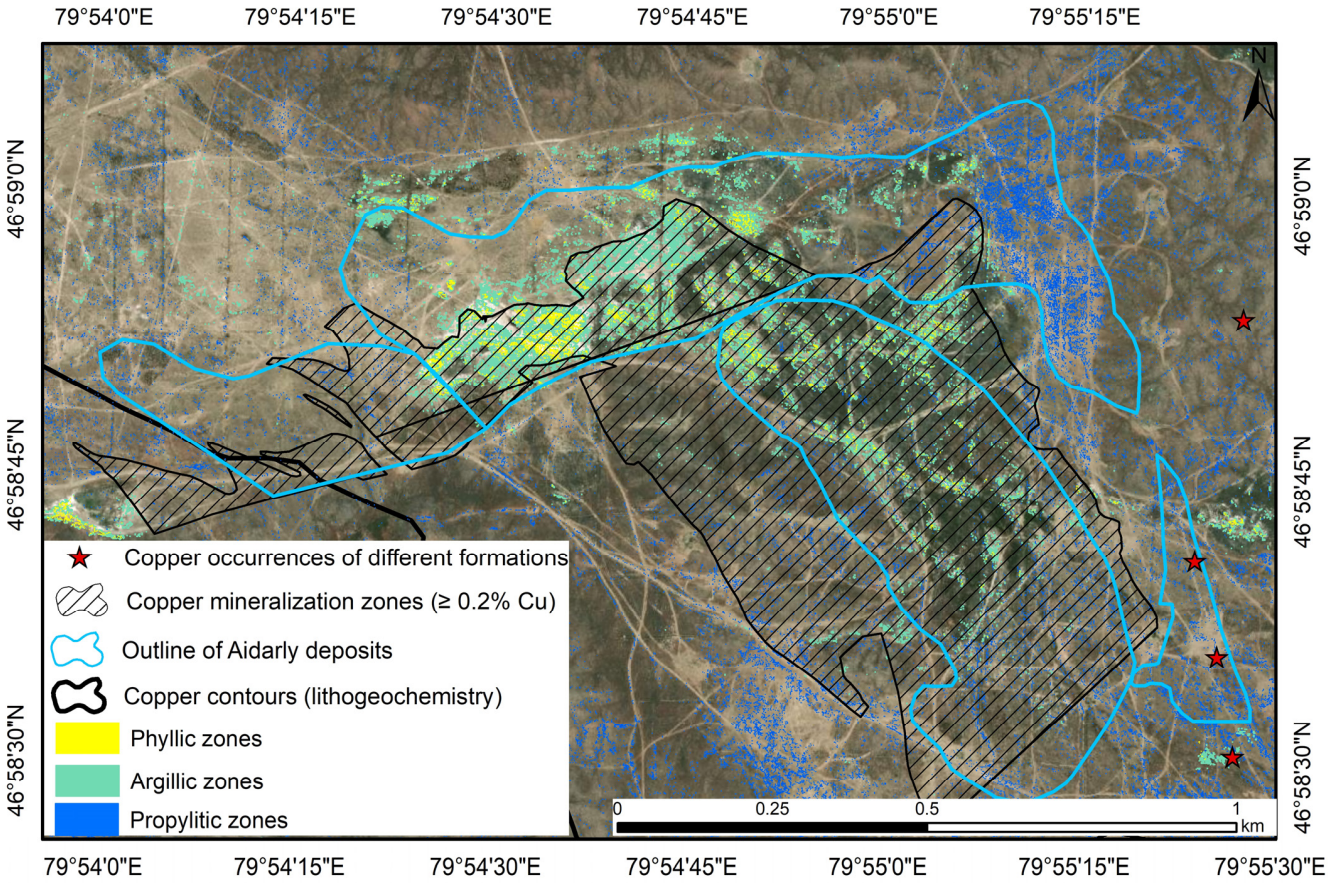


Figure 13. Overlay of interpreted hydrothermal alteration zones (WorldView-3) and the ore zone outline from the detailed geological map of the Aidarly deposit (following Krasnikov, A.M.).

A previously undocumented prospective zone was identified to the northwest of the Aidarly deposit. This area is characterized by a concentric zonation of phyllic and argillic alterations, clearly delineated using very high-resolution WorldView-3 imagery. A comparison with the lithogeochemical anomaly maps revealed a spatial correlation between the alteration zones and copper and bismuth anomalies, providing independent validation of the remote sensing interpretation (Figure 14). This spatial agreement highlights the geological relevance of the newly identified structure and suggests its potential as a target for further mineral exploration.

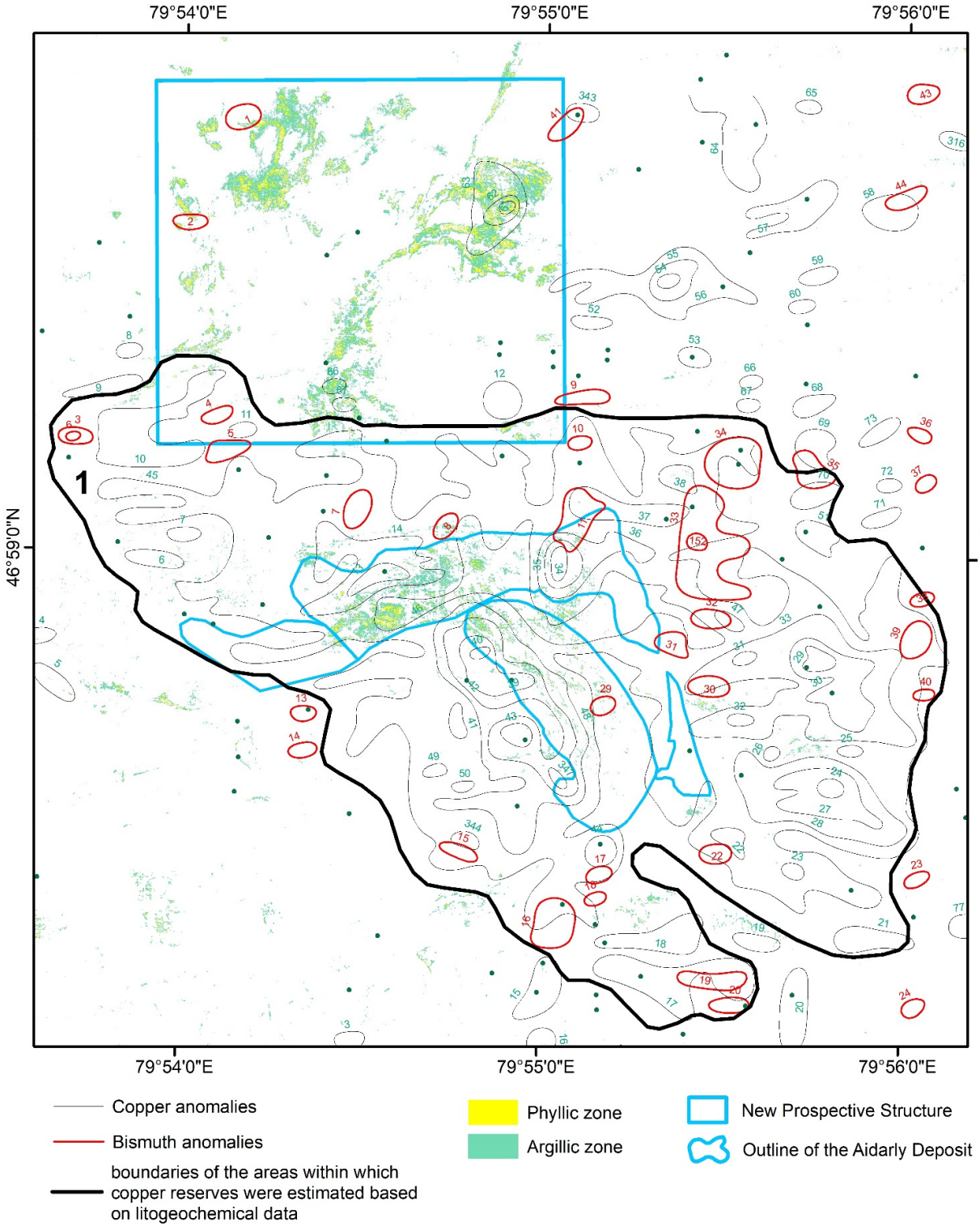


Figure 14. Spatial correlation between hydrothermal alteration zones and lithogeochemical anomalies.

5. Discussion

This study successfully mapped three main types of hydrothermal alteration—phyllic, argillic, and propylitic—across the Koldar area using ASTER data and a combination of the band ratio (BR), false color composite (FCC), and Spectral Angle Mapper (SAM) techniques (Figures 4, 5 and 7). The identified alteration zones are primarily concentrated in the northern and northwestern parts of the Koldar Massif. For more detailed analysis and verification, the Aidarly deposit was selected as a representative site due to its clear expression of alteration features. A high-resolution commercial WorldView-3 image was acquired for this purpose.

Unlike earlier studies [7,11,15,17,19,25], which primarily relied on medium-resolution satellite data for regional-scale mapping, this research introduces a multi-scale validation approach. The zones identified using ASTER were cross-verified with ultra-high-resolution WorldView-3 imagery, allowing for more accurate delineation of the alteration patterns at different spatial scales. This methodological approach combines datasets and their structured, scale-specific application: ASTER supports reconnaissance and regional targeting, while WorldView-3 enhances local validation and boundary precision. The advantage of this approach is particularly evident in complex terrains like the Koldar Massif, where abrupt lithological transitions and structural heterogeneity often blur signals in medium-resolution data.

The combination of the ASTER and WorldView-3 data with the BR, FCC, and SAM methods enabled effective multi-scale mapping of hydrothermal alterations. ASTER proved useful for regional targeting due to its spectral sensitivity in the SWIR range and moderate spatial resolution, though pixel mixing limited its detail. In contrast, WorldView-3 provided the precise delineation of alteration zones at a local scale but was limited by cost and spatial coverage. The complementarity between ASTER's regional reach and WorldView-3's detail represents a practical framework for mineral targeting, especially in underexplored terrains with restricted field access. Among the techniques, the SAM yielded the highest classification accuracy, particularly for phyllic zones; FCC provided strong visual interpretability; and BR was effective for targeting specific spectral features. Each method exhibited strengths depending on scale and objective, and their integration enhanced the overall mapping reliability. As a result of the comparative analysis of data obtained by the SAM method with the geological map of the study area, it was revealed that the hydrothermally altered zones identified on the ASTER and WorldView-3 data show a good correlation with the Aidarly ore zone, as well as a newly identified prospective zone (Figure 10). However, in the ASTER data, the hydrothermal zones were delineated in a coarser form and with less accuracy. In several areas where the WorldView-3 data clearly showed the presence of minerals associated with ore bodies, the ASTER data did not reveal these anomalies. This is due to the significantly higher pixel resolution of WorldView-3, which provides more detailed mapping and precise localization of alteration zones. Thus, using higher-resolution data, such as that from WorldView-3, allowed for better interpretation of geological structures and improved accuracy in delineating ore-bearing zones.

The spatial distribution of the detected alteration zones aligns well with the geological structure of the Koldar Massif. Phyllic and argillic alterations are concentrated along major tectonic structures, particularly in the northern and northwestern sectors, suggesting structural control over fluid flow. The strongest correlation between alteration zones and known copper mineralization was observed within the Aidarly deposit and surrounding areas. This supports the presence of a porphyry-type ore system, where zonation from phyllic to argillic alterations reflects thermal gradients and mineralization fronts. Lineament density analysis also indicates a genetic link between fracture systems and alteration

zones, highlighting the role of tectonics in ore localization. These findings contribute to a deeper understanding of the metallogenic framework of the region and improve targeting strategies.

The results underscore the strong potential of integrating ASTER and WorldView-3 data for mineral exploration in geologically complex terrains. The ability to delineate hydrothermal alteration zones that coincide with known copper occurrences confirms the reliability of these remote sensing methods for early-stage exploration. ASTER offers a cost-effective solution for broad-scale targeting, while WorldView-3 enables detailed local validation. The combined use of these tools can significantly reduce the area and cost of field investigations by narrowing down high-priority zones. Future exploration efforts in Kazakhstan and similar regions should focus on areas where phyllic and argillic alterations overlap with major structural features, as these are the most promising for mineralization.

To further enhance the precision and efficiency of mineral exploration, several improvements and field truth data are proposed. The integration of machine learning and data fusion techniques could significantly optimize the classification of alteration zones by combining multispectral, hyperspectral, geological, and geochemical datasets. Expanding the volume and diversity of ground truth data—particularly through systematic sampling and targeted field validation—would improve the accuracy of remote sensing interpretations. Additionally, future research could benefit from time series analysis of remote sensing data to monitor temporal changes in alteration patterns, potentially revealing active geological processes and refining exploration models.

6. Conclusions

The study demonstrates the effectiveness of combining ASTER and WorldView-3 data for mapping the hydrothermal alteration zones associated with porphyry copper mineralization. A multi-scale validation confirmed the geological relevance and reliability of remote sensing interpretations in the Koldar region. Three principal alteration zones—phyllic, argillic, and propylitic—were delineated across the Koldar Massif using the ASTER data. These zones are concentrated in the northern and northwestern parts of the massif and align with high lineament density areas, indicating structural control related to copper porphyry systems.

(1) A regional comparison with lithochemical data revealed a strong spatial correlation between the ASTER-derived alteration zones and geochemical anomalies, particularly near the Aidarly deposit, confirming the value of remote sensing-based predictions.
(2) The results of the alteration mapping using the ASTER data were validated against 22 copper occurrences representing different geological formations. Among the three tested methods—the Spectral Angle Mapper (SAM), false color composites (FCCs), and band ratios—all demonstrated a spatial correlation between the phyllic alteration zones and the occurrence points. The SAM achieved the highest validation accuracy (86.4%) and agreement ($\kappa = 0.73$), while FCCs and band ratios also produced consistent results. This confirms the reliability of ASTER-based mapping for detecting the alteration zones associated with various types of copper occurrences.
(3) The WorldView-3 imagery refined the spatial delineation of the alteration zones at Aidarly. The interpreted phyllic and argillic zones show a strong spatial correlation with the ore zone outline on the detailed geological map, confirming the utility of high-resolution data for accurately characterizing alteration at local scales.
(4) A previously undocumented structure was identified north of the main ore body. It shows spectral and structural features similar to the known mineralized zones. When compared with the lithochemical data, several areas within this zone correspond to

copper and bismuth anomalies. This newly identified area may serve as a promising target for further exploration.

This workflow can be applied to other underexplored regions with similar geological conditions. The integration of multispectral satellite data into early-stage mineral exploration improves targeting efficiency, reduces fieldwork costs, and supports data-driven decision-making. Future studies could enhance these methods through the use of machine learning for automated alteration mapping.

Author Contributions: Conceptualization, E.S. and K.T.; methodology, D.T.; software, E.O., A.B. and N.S.; validation, E.S.; formal analysis, E.O.; investigation, E.S.; resources, N.S. and A.B.; data curation, E.S.; writing—original draft preparation, E.S.; writing—review and editing, E.S. and K.T.; visualization, A.B.; supervision, E.S.; project administration, E.S.; and funding acquisition, E.S. All authors have read and agreed to the published version of the manuscript.

Funding: The research was funded by the Committee of Science of the Ministry of Science and Higher Education of the Republic of Kazakhstan (Grant No. BR21882179).

Data Availability Statement: The data are contained within the article.

Conflicts of Interest: The authors declare no conflicts of interest. The funders had no role in the design of the study; in the collection, analyses, or interpretation of data; in the writing of the manuscript; or in the decision to publish the results.

References

1. Sillitoe, R.H. Porphyry Copper Systems. *Econ. Geol.* **2010**, *105*, 3–41. [CrossRef]
2. Ragdanova, A.; Mataibayeva, I.; Frolova, O.; Agaliyeva, B.; Dolgopolova, A.; Togizov, K. Structural-formational zones with porphyry copper mineralization—A promising mineral resource base for copper in Eastern Kazakhstan. *Min. Miner. Depos.* **2025**, *19*, 107–120. [CrossRef]
3. Sabins, F.F. Remote sensing for mineral exploration. *Ore Geol. Rev.* **1999**, *14*, 157–183. [CrossRef]
4. Pour, A.B.; Hashim, M. The application of ASTER remote sensing data to porphyry copper and epithermal gold deposits. *Ore Geol. Rev.* **2012**, *44*, 1–9. [CrossRef]
5. Robb, L. *Introduction to Ore-Forming Processes*; Blackwell Publishing: Oxford, UK, 2004.
6. Pour, A.B.; Park, Y.; Park, T.-Y.S.; Hong, J.K.; Hashim, M.; Woo, J.; Ayoobi, I. Evaluation of ICA and CEM algorithms with Landsat-8/ASTER data for geological mapping in inaccessible regions. *Geocarto Int.* **2019**, *34*, 785–816. [CrossRef]
7. Bolatbekuly, S.; Umirova, G.; Zakariya, M.; Temirkhanova, R.; Togizov, K. Formation of prospecting criteria for copper-porphyry deposits based on the construction of reference models. *Nauk. Visnyk Natsionalnoho Hirnychoho Universytetu* **2024**, *2*, 19–24. [CrossRef]
8. Hunt, G.R.; Ashley, R.P. Spectra of altered rocks in the visible and near-infrared. *Econ. Geol.* **1979**, *74*, 1613–1629. [CrossRef]
9. Clark, R.N.; King, T.V.V.; Klejwa, M.; Swayze, G.; Vergo, N. High spectral resolution reflectance spectroscopy of minerals. *J. Geophys. Res.* **1990**, *95*, 12653–12680. [CrossRef]
10. Noori, L.; Pour, B.A.; Askari, G.; Taghipour, N.; Pradhan, B.; Lee, C.-W.; Honarmand, M. Comparison of different algorithms to map hydrothermal alteration zones using ASTER remote sensing data for polymetallic vein-type ore exploration: Toroud–Chahshirin Magmatic Belt (TCMB), North Iran. *Remote Sens.* **2019**, *11*, 495. [CrossRef]
11. Mars, J.C.; Rowan, L.C. Regional mapping of phyllic and argillic altered rocks in the Zagros magmatic arc, Iran, using ASTER data and logical operator algorithms. *Geosphere* **2006**, *2*, 161–186. [CrossRef]
12. Liu, L.; Zhou, J.; Jiang, D.; Zhuang, D.; Mansaray, L.R.; Zhang, B. Mineral resources prospecting by synthetic application of TM/ETM+, QuickBird and Hyperion data in the Hatu area, West Junggar, Xinjiang. *Sci. Rep.* **2017**, *6*, 21851. [CrossRef]
13. Pour, A.B.; Hashim, M. ASTER, ALI and Hyperion sensors data for lithological mapping and ore minerals exploration. *SpringerPlus* **2014**, *3*, 130. [CrossRef]
14. Bar, N.; Teleu, N.; Zlobin, H.; Mohr, P. Rock slope design and residual risk management for Aktogay Copper Mine, Kazakhstan. In Proceedings of the ISRM Congress, Salzburg, Austria, 9–14 October 2023.
15. Orynbassarova, E.; Ahmadi, H.; Adebiyet, B.; Bekbotayeva, A.; Abdullayeva, T.; Pour, A.B.; Ilyassova, A.; Serikbayeva, E.; Talgarbayeva, D.; Bermukhanova, A. Mapping Alteration Minerals Associated with Aktogay Porphyry Copper Mineralization in Eastern Kazakhstan Using Landsat-8 and ASTER Satellite Sensors. *Minerals* **2024**, *15*, 277. [CrossRef]

16. Liu, Y.; Sun, D.; Hu, X.; Ye, X.; Li, Y. Mapping alteration using imagery from the Tiangong-1 hyperspectral spaceborne system. *Int. J. Appl. Earth Obs. Geoinf.* **2018**, *64*, 275–286.
17. Carranza, E.J.M.; Hale, M. Mineral imaging with Landsat Thematic Mapper data for hydrothermal alteration mapping in heavily vegetated terrane. *Int. J. Remote Sens.* **2002**, *23*, 4827–4852. [CrossRef]
18. Pour, A.B.; Park, T.S.; Park, Y.; Hong, J.K.; Zoheir, B.; Pradhan, B.; Ayoobi, I.; Hashim, M. Application of multi-sensor satellite data for exploration of Zn-Pb sulfide mineralization in the Franklinian Basin, North Greenland. *Remote Sens.* **2018**, *10*, 1186. [CrossRef]
19. Pour, B.A.; Hashim, M.; van Genderen, J. Detection of hydrothermal alteration zones in a tropical region using satellite remote sensing data: Bau gold field, Sarawak, Malaysia. *Ore Geol. Rev.* **2013**, *54*, 181–196. [CrossRef]
20. Zoheir, B.; Emam, A.; Abdel-Wahed, M.; Soliman, N. Multispectral and radar data for the setting of gold mineralization in the South Eastern Desert, Egypt. *Remote Sens.* **2019**, *11*, 1450. [CrossRef]
21. Sirazhev, A.; Istekova, S.; Tolybaeva, D.; Togizov, K.; Temirkhanova, R. Methodology and results of detailed 3D seismic exploration in the Zhezkazgan Ore District. *Appl. Sci.* **2025**, *15*, 567. [CrossRef]
22. Gabr, S.S.; Hassan, S.M.; Sadek, M.F. Prospecting for new gold-bearing alteration zones at El-Hoteib area, South Eastern Desert, Egypt, using remote sensing data analysis. *Ore Geol. Rev.* **2015**, *71*, 1–13. [CrossRef]
23. Guha, A.; Yamaguchi, Y.; Chatterjee, S.; Rani, K.; Vinod Kumar, K. Emittance spectroscopy and broadband thermal remote sensing applied to phosphorite and its utility in geoexploration: A study in the parts of Rajasthan, India. *Remote Sens.* **2019**, *11*, 1003. [CrossRef]
24. Pour, A.B.; Hashim, M.; Hong, J.K.; Park, Y. Lithological and alteration mineral mapping in poorly exposed lithologies using Landsat-8 and ASTER satellite data: North-eastern Graham Land, Antarctic Peninsula. *Ore Geol. Rev.* **2019**, *108*, 112–133. [CrossRef]
25. Pour, A.B.; Hashim, M.; Park, Y.; Hong, J.K. Mapping alteration mineral zones and lithological units in Antarctic regions using spectral bands of ASTER remote sensing data. *Geocarto Int.* **2018**, *33*, 1281–1306. [CrossRef]
26. Amer, R.; El Mezayen, A.; Hasanein, M. ASTER spectral analysis for alteration minerals associated with gold mineralization. *Ore Geol. Rev.* **2016**, *75*, 239–251. [CrossRef]
27. Shahriari, H.; Ranjbar, H.; Honarmand, M. Image segmentation for hydrothermal alteration mapping using PCA and concentration–area fractal model. *Nat. Resour. Res.* **2013**, *22*, 191–206. [CrossRef]
28. Testa, F.J.; Villanueva, C.; Cooke, D.R.; Zhang, L. Lithological and hydrothermal alteration mapping of epithermal, porphyry and tourmaline breccia districts in the Argentine Andes using ASTER imagery. *Remote Sens.* **2018**, *10*, 203. [CrossRef]
29. Sheikhrahimi, A.; Pour, B.A.; Pradhan, B.; Zoheir, B. Mapping hydrothermal alteration zones and lineaments associated with orogenic gold mineralization using ASTER remote sensing data: A case study from the Sanandaj-Sirjan Zone, Iran. *Adv. Space Res.* **2019**, *63*, 3315–3332. [CrossRef]
30. Goetz, A.F.H.; Rock, B.N.; Rowan, L.C. Remote sensing for exploration: An overview. *Econ. Geol.* **1983**, *78*, 573–590. [CrossRef]
31. Zhao, Z.F.; Zhou, J.X.; Lu, Y.X.; Chen, Q.; Cao, X.M.; He, X.H.; Fu, X.H.; Zeng, S.H.; Feng, W.J. Mapping alteration minerals in the Pulang porphyry copper ore district, SW China, using ASTER and WorldView-3 data: Implications for exploration targeting. *Ore Geol. Rev.* **2021**, *134*, 104171. [CrossRef]
32. Ye, B.; Tian, S.; Ge, J.; Sun, Y. Assessment of WorldView-3 Data for Lithological Mapping. *Remote Sens.* **2017**, *9*, 1132. [CrossRef]
33. Hewson, R.D.; van der Werff, H.M.A.; Usman, M.S.; van der Meer, F.D.; Taranik, D.; Baugh, W. Worldview 3: Evaluation of its mineral mapping capability at Rodalquilar, Spain. In Proceedings of the 29th Annual Conference of the Geological Remote Sensing Group 2018, London, UK, 28–29 September 2018.
34. Bedini, E. Application of WorldView-3 imagery and ASTER TIR data to map alteration minerals associated with the Rodalquilar gold deposits, southeast Spain. *Adv. Space Res.* **2019**, *63*, 3346–3357. [CrossRef]
35. Kruse, F.A.; Perry, S.L. Mineral Mapping Using Simulated WorldView-3 Short-Wave Infrared Imagery. *Remote Sens.* **2013**, *5*, 2688–2703. [CrossRef]
36. Salehi, T.; Tangestani, M.H. Large-scale mapping of iron oxide and hydroxide minerals of Zefreh porphyry copper deposit, using Worldview-3 VNIR data in the Northeastern Isfahan, Iran. *Int. J. Appl. Earth Obs. Geoinf.* **2018**, *73*, 156–169. [CrossRef]
37. Kruse, F.A.; Baugh, M.W.; Perry, S.L. Validation of DigitalGlobe Worldview-3 earth imaging satellite shortwave infrared bands for mineral mapping. *J. Appl. Remote Sens.* **2015**, *9*, 096044. [CrossRef]
38. Cao, M.-J.; Li, G.-M.; Qin, K.-Z.; Evans, N.J.; Seitmuratova, E.Y. Assessing the magmatic affinity and petrogenesis of granitoids at the giant Aktogai porphyry Cu deposit, Central Kazakhstan. *Am. J. Sci.* **2016**, *316*, 614–668. [CrossRef]
39. Zvezdov, V.S.; Migachev, I.F.; Girfanov, M.M. Porphyry copper deposits of the CIS and the models of their formation. *Ore Geol. Rev.* **1993**, *7*, 511–549. [CrossRef]
40. Li, C.; Shen, P.; Pan, H.; Cao, C.; Seitmuratova, E. Geology and ore-forming fluid evolution of the Aktogai giant porphyry Cu deposit, Kazakhstan. *J. Asian Earth Sci.* **2018**, *165*, 192–209. [CrossRef]
41. NASA ASTER | Terra. Available online: https://terra.nasa.gov/about/terra-instruments/aster (accessed on 7 April 2022).
42. Abrams, M.; Hook, S.J. Simulated ASTER data for geologic studies. *IEEE Trans. Geosci. Remote Sens.* **1995**, *33*, 692–699. [CrossRef]

43. Asadzadeh, S.; Filho, C.R.S. Investigating the capability of WorldView-3 superspectral data for direct hydrocarbon detection. *Remote Sens. Environ.* **2016**, *173*, 162–173. [CrossRef]
44. Habashi, J.; Oskouei, M.M.; Moghadam, H.J.; Pour, A.B. Optimizing alteration mineral detection: A fusion of multispectral and hyperspectral remote sensing techniques in the Sar-e-Chah-e Shur, Iran. *Remote Sens. Appl. Soc. Environ.* **2024**, *35*, 101249. [CrossRef]
45. Lowell, J.D.; Guilbert, J.M. Lateral and Vertical Alteration-Mineralization Zoning in Porphyry Ore Deposits. *Econ. Geol.* **1970**, *65*, 373–408. Available online: https://www.scribd.com/document/423008513/Lowell-and-Guilbert-1970 (accessed on 11 August 2025). [CrossRef]
46. Ferrier, G.; White, K.; Griffiths, G.; Bryant, R.; Stefouli, M. The Mapping of Hydrothermal Alteration Zones on the Island of Lesvos, Greece Using an Integrated Remote Sensing Dataset. *Int. J. Remote Sens.* **2002**, *23*, 341–356. [CrossRef]
47. Abbaszadeh, M.; Hezarkhani, A. Hydrothermal Alteration Mapping Using ASTER Images in Parcam Area, Kerman. *J. Earth Sci.* **2010**, *78*, 123–128.
48. Khosravi, V.; Shirazi, A.; Shirazy, A.; Hezarkhani, A.; Pour, A.B. Hybrid Fuzzy-Analytic Hierarchy Process (AHP) Model for Porphyry Copper Prospecting in Simorgh Area, Eastern Lut Block of Iran. *Mining* **2021**, *2*, 1–12. [CrossRef]
49. Kamal El-Din, G.M.; El-Noby, E.; Abdelkareem, M.; Hamimi, Z. Using multispectral and radar remote sensing data for geological investigation, Qena-Safaga Shear Zone, Eastern Desert, Egypt. *Arab. J. Geosci.* **2021**, *14*, 997. [CrossRef]
50. Yazdi, Z.; Jafari Rad, A.; Aghazadeh, M.; Afzal, P. Alteration Mapping for Porphyry Copper Exploration Using ASTER and QuickBird Multispectral Images, Sonajeel Prospect, NW Iran. *J. Indian Soc. Remote Sens.* **2018**, *46*, 1581–1593. [CrossRef]
51. Kalinowski, A.; Oliver, S. ASTER mineral index processing manual. In *Remote Sensing Applications*; Internal Report No. 37; Geoscience: Symonston, Australia, 2004.
52. Horning, N. *Selecting the Appropriate Band Combination for an RGB Image Using Landsat Imagery Version 1.0*; American Museum of Natural History, Center for Biodiversity and Conservation: New York, NY, USA, 2004.
53. Fraser, S.J.; Green, A.A. A software defoliant for geological analysis of band ratios. *Int. J. Remote Sens.* **1987**, *8*, 525–532. [CrossRef]
54. Rowan, L.C.; Schmidt, R.G.; Mars, J.C. Distribution of hydrothermally altered rocks in the Reko Diq, Pakistan mineralized area based on spectral analysis of ASTER data. *Remote Sens. Environ.* **2006**, *104*, 74–87. [CrossRef]
55. Kruse, F.A.; Boardman, J.W.; Lefkoff, A.B.; Heidebrecht, K.B.; Shapiro, A.T.; Barloon, P.J.; Goetz, A.F.H. The Spectral Image Processing System (SIPS)—Interactive visualization and analysis of imaging spectrometer data. *Remote Sens. Environ.* **1993**, *44*, 145–163. [CrossRef]
56. Hasan, E.; Fagin, T.; El Alfy, Z.; Hong, Y. Spectral Angle Mapper and Aeromagnetic Data Integration for GoldAssociated Alteration Zone Mapping: A Case Study for the Central Eastern Desert Egypt. *Int. J. Remote Sens.* **2016**, *37*, 1762–1776. [CrossRef]
57. Shahriari, H.; Ranjbar, H.; Honarmand, M.; Carranza, E.J.M. Selection of less biased threshold angles for SAM classification using the real value—Area fractal technique. *Resour. Geol.* **2014**, *64*, 301–315. [CrossRef]
58. Shahriari, H.; Honarmand, M.; Ranjbar, H. Comparison of multi-temporal ASTER images for hydrothermal alteration mapping using a fractal-aided SAM method. *Int. J. Remote Sens.* **2015**, *36*, 1271–1289. [CrossRef]
59. Guha, A.; Kumar, K.V.; Rao, E.N.D.; Parveen, R. An image processing approach for converging ASTER-derived spectral maps for mapping Kolhan limestone, Jharkhand, India. *Curr. Sci.* **2014**, *106*, 40–49.
60. Abdelnasser, A.; Kumral, M.; Zoheir, B.; Karaman, M.; Weihed, P. REE geochemical characteristics and satellite-based mapping of hydrothermal alteration in Atud gold deposit, Egypt. *J. Afr. Earth Sci.* **2018**, *145*, 317–330. [CrossRef]
61. Meyer, C.; Hemley, J.J. Geochemistry of hydrothermal ore deposits. In *Wall-Rock Alteration*; Barnes, H.L., Ed.; Wiley: Hoboken, NJ, USA, 1967; pp. 166–235.
62. Khosroshahizadeh, S.; Pourkermani, M.; Almasian, M.; Arian, M.; Khakzad, A. Lineament Patterns and Mineralization Related to Alteration Zone by Using ASAR-ASTER Imagery in Hize Jan-Sharaf Abad Au-Ag Epithermal Mineralized Zone (East Azarbaijan—NW Iran). *Open J. Geol.* **2016**, *6*, 232–250. [CrossRef]
63. Ibrahim, W.S.; Watanabe, K.; Yonezu, K. Structural and litho-tectonic controls on Neoproterozoic base metal sulfide and gold mineralization in North Hamisana shear zone, South Eastern Desert, Egypt: The integrated field, structural, Landsat 7 ETM+ and ASTER data approach. *Ore Geol. Rev.* **2016**, *79*, 62–77. [CrossRef]
64. Pour, A.B.; Hashim, M. Identifying areas of high economic-potential copper mineralization using ASTER data in the Urumieh–Dokhtar Volcanic Belt, Iran. *Adv. Space Res.* **2012**, *49*, 753–769. [CrossRef]
65. El-Desoky, H.M.; Tende, A.W.; Abdel-Rahman, A.M.; Ene, A.; Awad, H.A.; Fahmy, W.; El-Awny, H.; Zakaly, H.M.H. Hydrothermal Alteration Mapping Using Landsat 8 and ASTER Data and Geochemical Characteristics of Precambrian Rocks in the Egyptian Shield: A Case Study from Abu Ghalaga, Southeastern Desert, Egypt. *Remote Sens.* **2022**, *14*, 3456. [CrossRef]
66. Available online: https://pubs.usgs.gov/of/2008/1321/pdf/OF081321_508.pdf (accessed on 11 August 2025).

67. Azizi, H.; Tarverdi, M.; Akbarpour, A. Extraction of hydrothermal alterations from ASTER SWIR data from east Zanjan, northern Iran. *Adv. Space Res.* **2010**, *46*, 99–109. [CrossRef]
68. Mahanta, P.; Maiti, S. Regional scale demarcation of alteration zone using ASTER imageries in South Purulia Shear Zone, East India: Implication for mineral exploration in vegetated regions. *Ore Geol. Rev.* **2018**, *102*, 846–861. [CrossRef]

Disclaimer/Publisher's Note: The statements, opinions and data contained in all publications are solely those of the individual author(s) and contributor(s) and not of MDPI and/or the editor(s). MDPI and/or the editor(s) disclaim responsibility for any injury to people or property resulting from any ideas, methods, instructions or products referred to in the content.